Article No. jmbi.1999.3378 available online at http://www.idealibrary.com on IDEAL® J. Mol. Biol. (2000) 295, 831–852

JMB

Kinetic Mechanism of the Single-stranded DNA Recognition by *Escherichia coli* Replicative Helicase DnaB Protein. Application of the Matrix Projection Operator Technique to Analyze Stopped-Flow Kinetics

Wlodzimierz Bujalowski* and Maria J. Jezewska

Department of Human Biological Chemistry and Genetics, The University of Texas Medical Branch at Galveston, 301 University Boulevard, Galveston, TX 77555-1053, USA

Kinetics of the *Escherichia coli* primary replicative helicase DnaB protein binding to a single-stranded DNA, in the presence of the ATP non-hydrolyzable analog AMP-PNP, have been performed, using the fluorescence stopped-flow technique. This is the first direct determination of the mechanism of the ssDNA recognition by a hexameric helicase. Binding of the fluorescent etheno-derivative of a ssDNA to the enzyme is characterized by a strong increase of the nucleic acid fluorescence, which provides an excellent signal to quantitatively study the mechanism of ssDNA recognition by the helicase. The kinetic experiments have been performed with a ssDNA 20-mer, $d\varepsilon A(p\varepsilon A)_{19}$, that encompasses the entire, total ssDNA-binding site of the helicase and with the 10-mer $d\varepsilon A(p\varepsilon A)_9$, which binds exclusively to the ssDNA strong subsite within the total ssDNA-binding site. Association of the DnaB helicase with the 20-mer is characterized by three relaxation times, which indicates that the binding occurs by the minimum three-step mechanism where the bimolecular binding step is followed by two isomerization steps. This mechanism is described by the equation:

$$\text{Helicase} + \text{ssDNA} \underset{k_{-1}}{\overset{k_1}{\leftrightarrow}} (\text{H-ssDNA})_1 \underset{k_{-2}}{\overset{k_2}{\leftrightarrow}} (\text{H-ssDNA})_2 \underset{k_{-3}}{\overset{k_3}{\leftrightarrow}} (\text{H-ssDNA})_3$$

The value of the bimolecular rate constant, k_1, is four to six orders of magnitude lower than the value expected for the diffusion-controlled reaction. Moreover, quantitative amplitude analysis suggests that the major conformational change of the ssDNA takes place in the formation of the $(\text{H-ssDNA})_1$. These results indicate that the determined first step includes formation of the collision and an additional transition of the protein-ssDNA complex, most probably the local opening of the protein hexamer. The data indicate that the binding mechanism reflects the interactions of the ssDNA predominantly through the strong ssDNA-binding subsite. The analysis of the stopped-flow kinetics has been performed using the matrix-projection operator technique, which provides a powerful method to address stopped-flow kinetics, particularly, the amplitudes. The method allowed us to determine the specific fluorescence changes accompanying the formation of all the intermediates. The sequential nature of the determined mechanism indicates the lack of the kinetically significant conformational equilibrium of the DnaB hexamer as well as a transient dissociation of the hexamer prior to the ssDNA binding. The significance of these results for the functioning of the DnaB helicase is discussed.

Keywords: helicase; DNA replication; protein-ssDNA interactions; stopped-flow kinetics

*Corresponding author

Abbreviation used: AMP-PNP, β,γ-imidoadenosine-5′-triphosphate.

E-mail address of the corresponding author: wbujalow@utmb.edu

0022-2836/00/040831–22 $35.00/0

Introduction

The DnaB protein is an essential replication protein in *Escherichia coli* that is involved in both the initiation and elongation stages of the chromosomal DNA replication, as well as in the replication of phage and plasmid DNA (Kornberg & Baker, 1992). The protein is the *E. coli* primary replicative helicase, i.e. the factor responsible for unwinding the duplex DNA in front of the replication fork (LeBowitz & McMacken, 1986; Baker *et al*., 1987; Kornberg & Baker, 1992). The DnaB protein is the only helicase required to reconstitute DNA replication *in vitro* from the chromosomal origin of replication (oriC). Multiple activities of the DnaB protein *in vitro* reflect complex interactions of the helicase with different ingredients in the primosome and in the protein-nucleic acid complexes that are formed at the origins of bacterial and phage DNA replication.

Sedimentation equilibrium, sedimentation velocity, and nucleotide cofactor binding studies show that the DnaB helicase exists as a stable hexamer in a large protein concentration range specifically stabilized by multiple magnesium cations (Bujalowski *et al*., 1994; Jezewska & Bujalowski, 1996b). Hydrodynamic and electron microscope data indicate that six protomers aggregate with cyclic symmetry in which the protomer-protomer contacts are limited to only two neighboring subunits (Bujalowski *et al*., 1994; San Martin *et al*., 1995; Yu *et al*., 1996). Thermodynamic studies provide direct evidence of the presence of long-range allosteric interactions in the hexamer encompassing all six subunits of the enzyme (Jezewska *et al*., 1996).

In the complex with the ssDNA, the DnaB helicase binds the nucleic acid with a stoichiometry of 20(±3) nucleotides per DnaB hexamer, and the formation of the DnaB-ssDNA complex does not require ATP hydrolysis (Bujalowski & Jezewska, 1995; Jezewska & Bujalowski, 1996a; Jezewska *et al*., 1996, 1997, 1998a,b,c). The helicase binds the ssDNA in a single orientation with respect to the polarity of the sugar-phosphate backbone of the nucleic acid (Jezewska *et al*., 1998a,b,c). This single orientation is preserved in the complexes of the enzyme with the replication fork. Photo-cross-linking experiments indicate that the ssDNA binds predominantly, if not completely, to a single subunit of the hexamer (Bujalowski & Jezewska, 1995; Jezewska *et al*., 1996). The DnaB hexamer has an effective, single binding site for the ssDNA, although each subunit can most probably be initially selected for ssDNA-binding. Our thermodynamic studies show that the total ssDNA-binding site of the enzyme is built of two subsites, a strong and a weak ssDNA-binding subsite, each of which encompasses a similar ~10 nucleotide residues each (Jezewska *et al*., 1998b,c). Moreover, fluorescence energy transfer studies indicate that in the complex with the helicase, the ssDNA passes through the cross-channel of the hexamer (Jezewska *et al*., 1998c).

Here, we address for the first time the mechanism of the DnaB helicase binding to the ssDNA using the fluorescence stopped-flow technique. Our data show that, in the presence of the ATP non-hydrolyzable analog, AMP-PNP, the association of the DnaB hexamer with the ssDNA proceeds through the minimum three-step sequential mechanism, where the bimolecular binding step is followed by two isomerization transitions. Amplitude analyses indicate that the major conformational transition of the protein-nucleic acid complex occurs in the first reaction step. These results and the lack of the effect of the protein concentration on the measured relaxation times indicate that the hexamer does not dissociate during DNA binding, and the entry of the ssDNA into the cross-channel of the hexamer occurs through a local opening of the ring-like structure. The sequential character of the reaction mechanism indicates that the ssDNA recognition by the DnaB hexamer is not preceded by a conformational transition of the helicase hexamer prior to DNA binding.

Results

General analysis of stopped-flow kinetic experiments using the matrix projection operator technique

A quantitative determination of the mechanism of the macromolecule-ligand interactions, using spectroscopic stopped-flow measurements, requires the examination of both the relaxation times and the amplitudes of the observed processes. In our analyses of the dynamics of the DnaB helicase-ssDNA interactions, we use the matrix projection operator technique (Pilar, 1968). This very powerful approach, familiar in the field of quantum chemistry, has so far been used very little in chemical kinetics where standard matrix methods are applied (Bernasconi, 1976). As we show below, the matrix projection operator technique is extremely useful for the analysis of complex stopped-flow kinetics, particularly, by providing closed-form expressions for the amplitudes of the studied reaction. This, in turn, allows the experimenter to obtain structural mechanistic information about all identified intermediates.

Our data show that the formation of the DnaB helicase complex with the ssDNA includes the bimolecular step leading to the formation of the initial complex, which subsequently undergoes several first-order conformational transitions. Therefore, as an example, we consider a complex sequential reaction between ligand, C, and protein, N, of the type:

$$C_1 + N_1 \underset{k_{-1}}{\overset{k_1}{\rightleftharpoons}} N_2 \underset{k_{-2}}{\overset{k_2}{\rightleftharpoons}} N_3 \underset{k_{-3}}{\overset{k_3}{\rightleftharpoons}} N_4 \qquad (1)$$

where the initial bimolecular process is followed by two isomerization reactions of the formed complex and the reaction is monitored by the ligand

fluorescence change. This reaction is characterized by three relaxation times and three amplitudes, i.e. there are three normal modes of the reaction (Bernasconi, 1976). The differential equations describing the time-course of reaction (1), in terms of different macromolecule species, are:

$$\begin{aligned}\frac{dN_1}{dt} &= -k_1N_1C + k_{-1}N_2\\ \frac{dN_2}{dt} &= k_1N_1C - (k_{-1}+k_2)N_2 + k_{-2}N_3\\ \frac{dN_3}{dt} &= k_2N_2 - (k_{-2}+k_3)N_2 + k_{-3}N_4\\ \frac{dN_4}{dt} &= k_3N_3 - k_{-3}N_4\end{aligned} \tag{2}$$

In order to eliminate all higher-order terms in differential equations and to formulate the kinetic mechanism, our kinetic studies are performed in pseudo-first-order conditions, i.e. in the large excess of the ligand, $C_{tot} \gg N_{tot}$, i.e. C_{tot} is $\sim$ constant during the reaction. In matrix notation, system (2) is then defined as:

$$\begin{pmatrix}\frac{dN_1}{dt}\\ \frac{dN_2}{dt}\\ \frac{dN_3}{dt}\\ \frac{dN_4}{dt}\end{pmatrix} = \begin{pmatrix}-k_1C & k_{-1} & 0 & 0\\ k_1C & -(k_{-1}+k_2) & k_{-2} & 0\\ 0 & k_2 & -(k_{-2}+k_3) & k_3\\ 0 & 0 & k_3 & -k_3\end{pmatrix}\begin{pmatrix}N_1\\ N_2\\ N_3\\ N_4\end{pmatrix} \tag{3}$$

and:

$$\dot{\mathbf{N}} = \mathbf{M}\mathbf{N} \tag{4}$$

where $\dot{\mathbf{N}}$ is a vector of time derivatives, $\mathbf{M}$ is the coefficient matrix, and $\mathbf{N}$ is a vector of concentrations. In standard matrix approach the solution of system (3) is:

$$\mathbf{N} = \exp(\mathbf{M}t)\mathbf{N_o} \tag{5}$$

and:

$$\mathbf{N} = \mathbf{V}\begin{pmatrix}\exp(\lambda_0 t) & 0 & 0 & 0\\ 0 & \exp(\lambda_1 t) & 0 & 0\\ 0 & 0 & \exp(\lambda_2 t) & 0\\ 0 & 0 & 0 & \exp(\lambda_3 t)\end{pmatrix}\mathbf{V}^{-1}\mathbf{N_o} \tag{6}$$

where λ_0, λ_1, λ_2, and λ_3 are eigenvalues of matrix $\mathbf{M}$, $\mathbf{V}$ is a matrix whose columns are the eigenvectors of matrix $\mathbf{M}$, and $\mathbf{N_o}$ is the vector of the initial concentrations. In the considered case of the sequential reaction 1, $\mathbf{N_o}$ is a column vector (N_{tot}, 0, 0, 0), where N_{tot} is the total concentration of macromolecule N. The form of the vector $\mathbf{N_o}$ reflects the fact that at $t = 0$ the concentration of the free macromolecule is equal to its total concentration, while the concentrations of all other species are zero. In order to solve system (3), i.e. find relaxation times and amplitudes of the reaction, first one has to obtain the eigenvalues of matrix $\mathbf{M}$, then the corresponding eigenvectors. For a multistep mechanism, like that considered here, this can be achieved only through cumbersome numerical analyses, particularly for the eigenvectors, without obtaining information about the spectroscopic (structural) information about each intermediate.

However, instead of finding eigenvectors corresponding to each eigenvalue, λ_i, of matrix $\mathbf{M}$, we expanded the matrix $\exp(\mathbf{M}t)$ using its eigenvalues, $\exp(\lambda_i t)$, and corresponding projection operators, $\mathbf{Q}_i$, as (Fraser *et al.*, 1965; Pilar, 1968):

$$\exp(\mathbf{M}t) = \sum_{i=0}^{3}\mathbf{Q}_i\exp(\lambda_i t) \tag{7}$$

The projection operators, $\mathbf{Q}_i$, can easily be defined by Sylvester's theorem, using the original coefficient matrix $\mathbf{M}$ and its eigenvalues, λ_i (Fraser *et al.*, 1965; Pilar, 1968). In general, a projection operator, $\mathbf{Q}_i$, corresponding to an eigenvalue, λ_i, is:

$$\mathbf{Q}_i = \frac{\prod_{j\neq i}^{n}(\mathbf{M} - \lambda_j\mathbf{I})}{\prod_{j\neq i}^{n}(\lambda_i - \lambda_j)} \tag{8}$$

where n is the number of eigenvalues and $\mathbf{I}$ is the identity matrix of the same size as $\mathbf{M}$.

In the considered reaction, which includes three sequential steps (equation (1)), there are four eigenvalues λ_0, λ_1, λ_2, and λ_3, however, $\lambda_0 = 0$ because of the mass conservation in the reaction system. Therefore, using equation (8) one obtains:

$$\mathbf{Q}_0 = \frac{(\mathbf{M} - \lambda_1\mathbf{I})(\mathbf{M} - \lambda_2\mathbf{I})(\mathbf{M} - \lambda_3\mathbf{I})}{\lambda_1\lambda_2\lambda_3} \tag{9a}$$

$$\mathbf{Q}_1 = \frac{\mathbf{M}(\mathbf{M} - \lambda_2\mathbf{I})(\mathbf{M} - \lambda_3\mathbf{I})}{\lambda_1(\lambda_1 - \lambda_2)(\lambda_1 - \lambda_3)} \tag{9b}$$

$$\mathbf{Q}_2 = \frac{\mathbf{M}(\mathbf{M} - \lambda_1\mathbf{I})(\mathbf{M} - \lambda_3\mathbf{I})}{\lambda_2(\lambda_2 - \lambda_1)(\lambda_2 - \lambda_3)} \tag{9c}$$

$$\mathbf{Q}_3 = \frac{\mathbf{M}(\mathbf{M} - \lambda_1\mathbf{I})(\mathbf{M} - \lambda_2\mathbf{I})}{\lambda_3(\lambda_3 - \lambda_1)(\lambda_3 - \lambda_2)} \tag{9d}$$

The solution of the system of the differential equation (equation (5)), expressed in terms of matrix projection operators, is then:

$$\mathbf{N} = \mathbf{Q}_0\mathbf{N_o} + \mathbf{Q}_1\mathbf{N_o}\exp(\lambda_1 t) + \mathbf{Q}_2\mathbf{N_o}\exp(\lambda_2 t) + \mathbf{Q}_3\mathbf{N_o}\exp(\lambda_3 t) \tag{10}$$

where $\mathbf{Q}_i$ are defined by equations (9).

Using matrix projection operators, the numerical analysis of the complex multi-step reaction is reduced to finding only the eigenvalues of the original coefficient matrix **M**. As we show below, the power of this technique is particularly evident in obtaining closed-form formulas for amplitudes of different normal modes of the reaction in terms of rate constants, relaxation times, and spectroscopic properties of each intermediate.

Inspection of equations (9) and their comparison with equation (10) show that projection operators, $\mathbf{Q}_i$, are matrices of the same size as the size of the original coefficient matrix **M**. Also, the products $\mathbf{Q}_i\mathbf{N_o}$ are column vectors, $\mathbf{P}_i$, which are the projections of $\mathbf{N_o}$ on each eigenvector of the matrix **M**. Notice, that $\mathbf{P}_i$ are obtained without determining the eigenvectors of **M**. Thus:

$$\mathbf{N} = \mathbf{P}_0 + \mathbf{P}_1\exp(\lambda_1 t) + \mathbf{P}_2\exp(\lambda_2 t) + \mathbf{P}_3\exp(\lambda_3 t) \tag{11a}$$

and:

$$\begin{pmatrix} N_1 \\ N_2 \\ N_3 \\ N_4 \end{pmatrix} = \begin{pmatrix} P_{01} \\ P_{02} \\ P_{03} \\ P_{04} \end{pmatrix} + \begin{pmatrix} P_{11} \\ P_{12} \\ P_{13} \\ P_{14} \end{pmatrix}\exp(\lambda_1 t) + \begin{pmatrix} P_{21} \\ P_{22} \\ P_{23} \\ P_{24} \end{pmatrix}\exp(\lambda_2 t) + \begin{pmatrix} P_{31} \\ P_{32} \\ P_{33} \\ P_{34} \end{pmatrix}\exp(\lambda_3 t) \tag{11b}$$

where P_{ij} is the jth element of the projection of the vector of the initial concentrations $\mathbf{N_o}$ on the eigenvector, corresponding to the ith eigenvalue of matrix **M**. In stopped-flow experiments, the concentrations of all macromolecule species change from the concentrations at $t = 0$ to the equilibrium concentrations at $t = \infty$ defined by the elements of vector $\mathbf{P}_0$. It should be pointed out that each element of P_{ij} in equation (11b) is an algebraic expression, in term of eigenvalues, λ_i, rate constants of the system, and total ligand and macromolecule concentrations, defined by the products $\mathbf{Q}_i\mathbf{N}_o$.

There are three normal modes of the reaction and three amplitudes, A_1, A_2, and A_3, corresponding to relaxation times $\tau_1 = -1/\lambda_1$, $\tau_2 = -1/\lambda_2$, and $\tau_3 = -1/\lambda_3$. In spectroscopic stopped-flow experiments, concentrations of the reactants and products are indirectly monitored through some spectroscopic parameter (e.g. fluorescence), characterizing interacting species. In general, each intermediate will have different fluorescence properties. Thus, there are four molar fluorescence intensities, F_1, F_2, F_3, and F_4, characterizing C_1, N_2, N_3, and N_4 states of the ligand, free and in the complex with the macromolecule. The concentrations of all ligand species, at any time of the reaction, follow the mass conservation relationship:

$$C_{\text{tot}} = C_1 + N_2 + N_3 + N_4 \tag{12}$$

where N_2, N_3 and N_4 are defined by equation (11b).

The fluorescence of the system at time t of the reaction, $F(t)$, is defined by:

$$F(t) = F_1C_1 + F_2N_2 + F_3N_3 + F_4N_4 \tag{13}$$

Introducing equations (11b) and (12) into equation (13), one obtains:

$$F(t) = F_1C_1 + \begin{pmatrix} F_2P_{02} + F_3P_{03} + F_4P_{04} \\ F_2P_{13} + F_3P_{13} + F_4P_{14} \\ F_2P_{22} + F_3P_{23} + F_4P_{24} \\ F_2P_{32} + F_3P_{33} + F_4P_{34} \end{pmatrix}^{\mathrm{T}} \begin{pmatrix} 1 \\ \exp(\lambda_1 t) \\ \exp(\lambda_2 t) \\ \exp(\lambda_3 t) \end{pmatrix} \tag{14}$$

where index T indicates the transpose matrix. The observed total amplitude, A_{tot} of the stopped-flow trace is the sum of individual amplitudes of all normal modes:

$$A_{\text{tot}} = A_1 + A_2 + A_3 \tag{15a}$$

Experimentally, for any stopped-flow trace the total amplitude, A_{tot} is described by:

$$A_{\text{tot}} = F(0) - F(\infty) \tag{15b}$$

where $F(0)$ and $F(\infty)$) are the observed fluorescence intensities, $F(t)$, of the system at $t = 0$ and $t = \infty$, respectively. Introducing the mass conservation relationship defined by equation (12) into equation (14), $t = 0$ for $F(0)$ and $t = \infty$ for $F(\infty)$, one obtains:

$$F(0) = F_1C_{\text{tot}} + (P_{02} + P_{12} + P_{22} + P_{32} \quad P_{03} + P_{13} + P_{23} + P_{33} \quad P_{04} + P_{14} + P_{24} + P_{34}) \begin{pmatrix} F_2 - F_1 \\ F_3 - F_1 \\ F_4 - F_1 \end{pmatrix} \tag{16}$$

and:

$$F(\infty) = F_1 C_{\text{tot}} + (P_{02} \quad P_{03} \quad P_{04}) \begin{pmatrix} F_2 - F_1 \\ F_3 - F_1 \\ F_4 - F_1 \end{pmatrix} \quad (17)$$

which define the total amplitude (equation (15b)) as:

$$A_{\text{tot}} = (P_{12} + P_{13} + P_{14} \quad P_{22} + P_{23} + P_{24} \quad P_{32} + P_{33} + P_{34}) \begin{pmatrix} F_2 - F_1 \\ F_3 - F_1 \\ F_4 - F_1 \end{pmatrix} \quad (18)$$

The individual amplitudes A_1, A_2, and A_3 for each normal mode are then:

$$A_1 = (P_{12} \quad P_{13} \quad P_{14}) \begin{pmatrix} F_2 - F_1 \\ F_3 - F_1 \\ F_4 - F_1 \end{pmatrix} \quad (19)$$

$$A_2 = (P_{22} \quad P_{23} \quad P_{24}) \begin{pmatrix} F_2 - F_1 \\ F_3 - F_1 \\ F_4 - F_1 \end{pmatrix} \quad (20)$$

$$A_3 = (P_{32} \quad P_{33} \quad P_{34}) \begin{pmatrix} F_2 - F_1 \\ F_3 - F_1 \\ F_4 - F_1 \end{pmatrix} \quad (21)$$

Equations (18)-(21) are closed-form, explicit expressions for the total and individual amplitudes for the three-step reaction mechanism described by equation (1). Thus, once the matrix operators are formulated in terms of the original matrix of coefficients **M**, the total and individual amplitudes of the reaction system can be defined easily. Extension of the analysis to more complex reaction systems is straightforward.

The relationships derived above also provide an important intuitive insight into the effect of different values of spectroscopic properties of the intermediates of the reaction on observed amplitudes. For instance, even if all intermediates have the same fluorescence properties ($F_2 = F_3 = F_4$), the amplitudes of all normal modes will be observed, in spite of the fact that there are no additional fluorescence changes in all transitions following N_2. Equations (18)-(21) show that the dominant factors affecting the individual amplitudes are the differences between the fluorescence of the free ligand and a given intermediate and not the progressive fluorescence changes in subsequent transitions. For some kinetic system, it may not be possible to detect all present, normal modes of the reaction (Bernasconi, 1976; Bujalowski *et al.*, 1986a). However, this would result from the combined effect of rate constants, relaxation times and spectroscopic changes and not from similar or identical spectroscopic signal changes accompanying the formation of subsequent intermediates. The equations derived here are for the case where the observed spectroscopic signal (fluorescence) originates from the ligand. Analogous equations can easily be obtained when the observed signal comes from the macromolecule.

The obtained expressions for the individual amplitudes of the kinetic steps make it possible to extract the spectroscopic properties of each intermediate of the reaction, thus, providing information about the structure of the intermediate, unavailable by other methods. Notice, this can be facilitated by setting the fluorescence of the free ligand, $F_1 = 1$. Then, all remaining molar fluorescence intensities, F_2, F_3, and F_4 are uniquely determined, relative to F_1, by equations (18)-(21). However, in practice, due to experimental error, the determination of F_2, F_3, and F_4 can be obtained through non-linear least-squares fitting of the experimentally obtained individual amplitudes. Because the quantum yield for the free ligand can be obtained independently, then, if required, the true quantum yields for all other intermediates can also be determined.

Relaxation times

Examination of the relaxation times of the studied kinetics, as a function of the ligand concentration, constitutes the first and fundamental step in establishing the mechanism of the complex reaction and the rate constants of particular elementary processes (Bernasconi, 1976). The reciprocal relaxation times for the three-step sequential reaction, described by equation (1), as a function of the free ligand concentration are shown in Figure 1(a)-(c). Relaxation times have been obtained by direct, numerical determination of the eigenvalues, λ_1, λ_2, and λ_3 of the matrix **M**, at a given free ligand concentration, C_1, using the identities of $1/\tau_1 = -\lambda_1$, $1/\tau_2 = -\lambda_2$, and $1/\tau_3 = -\lambda_3$. The selected rate constants are: $k_1 = 1 \times 10^5$ M^{-1} s^{-1}, $k_{-1} = 0.05$ s^{-1}, $k_2 = 0.1$ s^{-1}, $k_{-2} = 0.05$ s^{-1}, $k_3 = 0.01$ s^{-1}, and $k_{-3} = 0.005$ s^{-1}. Because of the large differences between the values of the selected rate constants among the elementary steps, the relaxation times differ significantly at any concentration of the ligand, i.e. the normal modes of the reaction are close to the ''uncoupled'' ones (Bernasconi, 1976). In such a situation, it could be possible to obtain approximate formulas for each of the relaxation times; however, the numerical approach applied here avoids such approximations. The largest reciprocal relaxation time has typical characteristics of the bimolecular binding process with $1/\tau_1$ increasing linearly with the ligand concentration in the high ligand concentration range (Bernasconi, 1976). On the other hand, at low ligand concentrations there is clearly a non-linear region. This non-linear region, observed experimentally (see below), is evident only because no approximate expression for this relaxation time is used. Both $1/\tau_2$ and $1/\tau_3$ for the considered sequential three-step

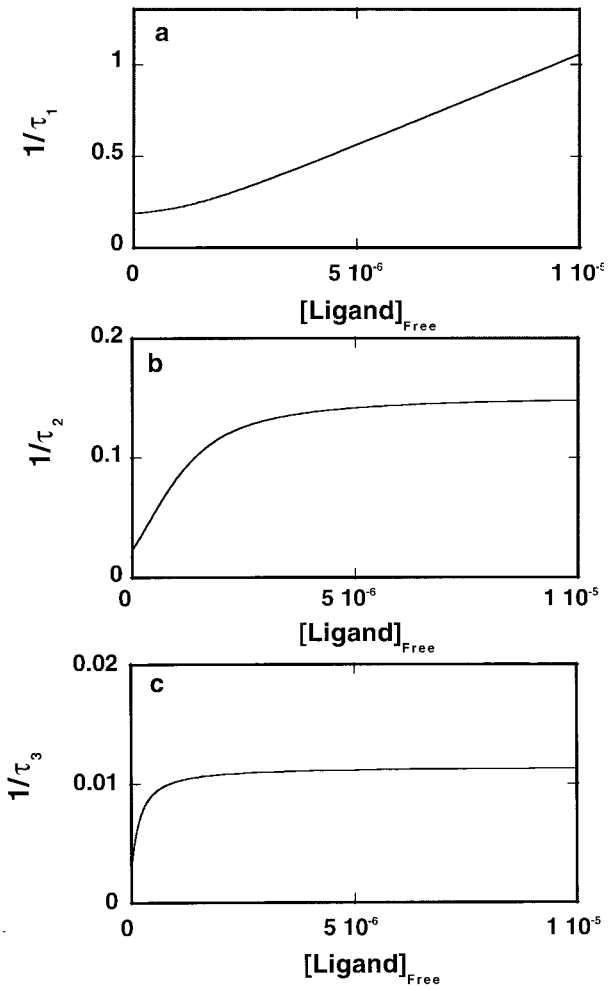

Figure 1. Computer simulation of the dependence of reciprocal relaxation times for the three-step sequential mechanism of the ligand binding to a macromolecule, defined by equation (1), upon free ligand concentration. Relaxation times have been obtained by numerically determining the eigenvalues of the matrix of coefficient **M** (λ_1, λ_2, λ_3) and using identities: $1/\tau_1 = -\lambda_1$, $1/\tau_2 = -\lambda_2$, and $1/\tau_3 = -\lambda_3$. The simulations have been performed using rate constants: $k_1 = 1 \times 10^5$ M^{-1} s^{-1}, $k_{-1} = 0.05$ s^{-1}, $k_2 = 0.1$ s^{-1}, $k_{-2} = 0.05$ s^{-1}, $k_3 = 0.01$ s^{-1}, and $k_{-3} = 0.005$ s^{-1}. The selected total ligand, C_{tot}, and macromolecule, N_{tot}, concentrations are 1×10^{-5} M and 1×10^{-8} M, respectively; (a) $1/\tau_1$, (b) $1/\tau_2$, (c) $1/\tau_3$.

reaction show hyperbolic dependence upon [ligand] reaching the plateau values at high [ligand]. As a result, τ_2 and τ_3 become independent of the ligand concentration in the high concentration range. It should be pointed out that $1/\tau_3$ reaches the plateau value at significantly lower ligand concentrations than $1/\tau_2$. The hyperbolic dependence of $1/\tau_3$ upon [ligand] is often unnoticed, particularly under pseudo-first-order conditions.

Amplitudes

Analysis of the amplitudes of the spectroscopic relaxation process offers a unique opportunity to obtain information about the structure of the reaction intermediates and the physical nature of the elementary steps. The dependence of individual amplitudes A_1, A_2, and A_3, expressed as fractions of the total amplitude A_{tot}, $(A_i/\Sigma A_i)$ upon the ligand concentration, is shown in Figure 2. The total amplitude, A_{tot}, normalized to 1 at high ligand concentrations is included. The computer simulations have been performed using equations (18)-(21). The selected molar fluorescence intensities are $F_1 = 1$, $F_2 = 3$, $F_3 = 3.5$, and $F_4 = 3.5$; the rate constants are the same as in Figure 1. It is clear that at low ligand concentrations only the amplitudes of the second, A_2, and third, A_3, normal modes of the reaction contribute significantly to the observed A_{tot}, although a major fluorescence change, as compared to the fluorescence of the free ligand, accompanies the formation of N_2. Such behavior is the result of the low efficiency of the N_2 complex formation at low [ligand], while the formed complex still relaxes with the second and third normal mode. At high ligand concentrations, the amplitude of the first normal mode, A_1, dominates the relaxation process. The computer simulations in Figure 2 show that all three amplitudes of the present relaxation steps are detectable, in spite of the fact that there is no additional fluorescence change in the transition from N_3 to N_4. As mentioned above, this is evident from equations (19)-(21), which show that an amplitude for a

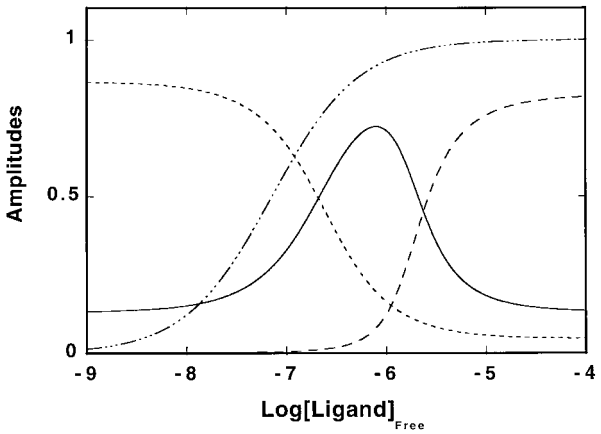

Figure 2. Computer simulation of the dependence of individual, A_1, A_2, and A_3, and the total, A_{tot}, relaxation amplitudes for the three-step sequential mechanism of a ligand binding to a macromolecule, defined by equation (1), upon the logarithm of the free ligand concentration. The relative fluorescence intensities, F_2, F_3, and F_4, characterizing corresponding intermediates, N_2, N_3, and N_4, are 3, 3.5 and 3.5, respectively. The fluorescence of the free ligand, C_1, is taken as 1. The individual amplitudes are expressed as fractions of the total amplitude A_{tot}, while the total amplitude has been normalized to 1 at saturating ligand concentrations. The simulations have been performed using closed-form expressions defined by equations (18)-(21) with the rate constants: $k_1 = 1 \times 10^5$ M^{-1} s^{-1}, $k_{-1} = 0.05$ s^{-1}, $k_2 = 0.1$ s^{-1}, $k_{-2} = 0.05$ s^{-1}, $k_3 = 0.01$ s^{-1}, and $k_{-3} = 0.005$ s^{-1}; A_1 (– – –), A_2 (—), A_3 (- - -), A_{tot} (— - - - —).

given normal mode of the reaction is mainly affected by the difference between the spectroscopic properties of intermediates and the free ligand (see above).

Computer simulations shown in Figure 2 were performed with given values of the relative fluorescence intensities for all intermediates. In experimental studies of a kinetic system this process is reversed, i.e. from the dependence of the amplitudes of the system upon ligand (or macromolecule) concentrations one can determine the spectroscopic parameters characterizing all intermediates, as we discuss below, for the case of the DnaB association with ssDNA oligomers.

Kinetics of the 20-mer, dεA(pεA)$_{19}$, binding to the DnaB helicase

The site-size of the DnaB hexamer in the complex with the ssDNA is 20(±3) nucleotide residues per hexamer, independent of the type of the base (Bujalowski & Jezewska, 1995; Jezewska & Bujalowski, 1996a; Jezewska *et al*., 1996). The DnaB hexamer binds a single 20-mer molecule and the oligomer encompasses the entire total binding site of the helicase. As we have shown before, binding of the fluorescent etheno-derivative of dA(pA)$_{19}$, dεA(pεA)$_{19}$, is accompanied by a strong, ~3-fold, increase of the nucleic acid fluorescence, providing an excellent signal to monitor the kinetics of the helicase-ssDNA complex formation (Bujalowski & Jezewska, 1995). The stopped-flow experiments have been performed under pseudo-first-order conditions by mixing the DnaB helicase with a large excess of the 20-mer. At the concentration used (1.5×10^{-7} M hexamer), the DnaB helicase fully preserves its hexameric structure (Bujalowski *et al*., 1994a,b; Jezewska & Bujalowski, 1996a,b). The stopped-flow kinetic trace of the dεA(pεA)$_{19}$ fluorescence, after mixing 5×10^{-6} M oligomer with 1.5×10^{-7} M hexamer DnaB helicase (final concentrations) in buffer T2 (pH 8.1, 100 mM NaCl, 1 mM AMP-PNP, 10°C), is shown in Figure 3. The curve is shown in two time bases, ten seconds and 1000 seconds. The observed kinetics is complex, clearly showing the presence of multiple steps. The continuous line in Figure 3 is a non-linear least-squares fit of the experimental curve using a three-exponential fit. As indicated by the included deviations of the experimental curve from the fit, the two-exponential function provides a less than adequate description of the experimentally observed kinetics. Thus, the three-exponential fit is necessary to represent the observed experimental curve. A higher number of exponents does not significantly improve the statistics of the fit. Therefore, the association of the ssDNA 20-mer with the total binding site of the DnaB helicase is a complex process that includes at least three steps. It is interesting to note that the observed kinetics of the ssDNA 20-mer binding to the DnaB helicase is relatively slow (Figure 3). The entire kinetic process takes ~17 minutes to reach equilibrium. Also, the rate depends little on the temperature (data not shown). Notice, at this high concentration of the 20-mer only ~50% of the total amplitude is included in the first ten seconds of the reaction time.

The reciprocal relaxation times, $1/\tau_1$, $1/\tau_2$, and $1/\tau_3$, characterizing the three binding steps, as a function of the total dεA(pεA)$_{19}$ concentration are shown in Figures 4(a)-(c). The largest reciprocal time, $1/\tau_1$, increases with [dεA(pεA)$_{19}$] and the

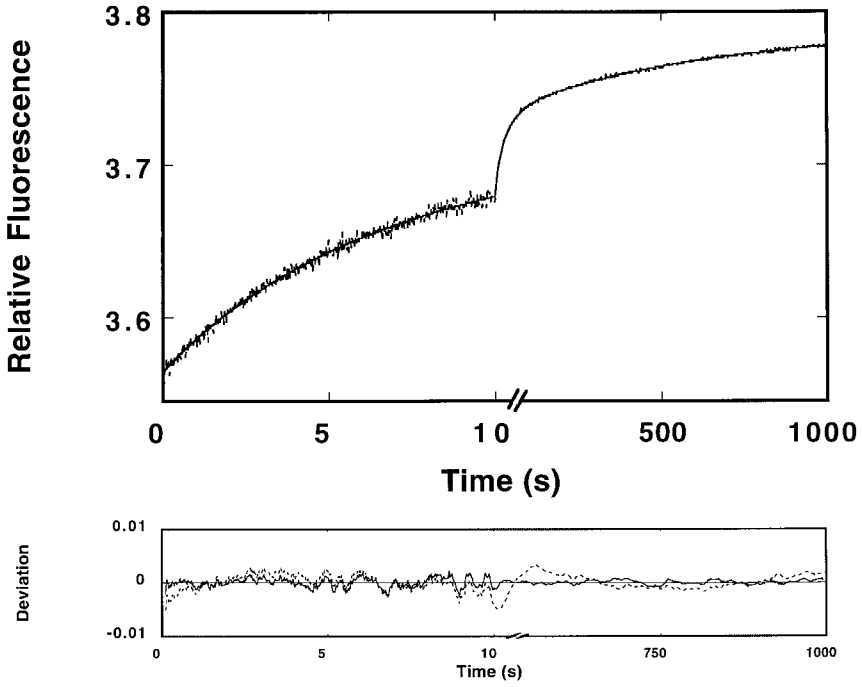

Figure 3. The top panel is the fluorescence stopped-flow kinetic trace, recorded in two time bases, ten seconds and 1000 seconds, after mixing the DnaB helicase with the 20-mer, dεA(pεA)$_{19}$ in buffer T2 (pH 8.1, 100 NaCl, 1 mM AMP-PNP) ($\lambda_{ex} = 320$ nm, $\lambda_{em} > 400$ nm). The final concentrations of the helicase and the 20-mer are 1.5×10^{-7} M hexamer and 5×10^{-6} M oligomer, respectively. The continuous line is the three-exponential, non-linear least-squares fit of the experimental curve using equation (26). The lower panel shows the deviations of the experimental curve from the fit using the two-exponential (broken line) and three-exponential (continuous line) functions (equation (26)), respectively.

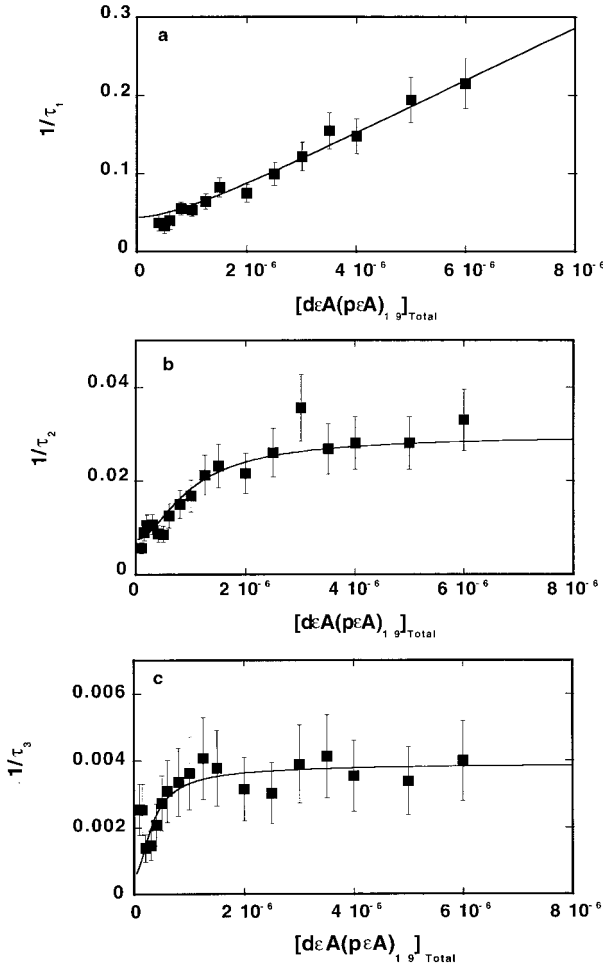

Figure 4. The dependence of the reciprocal of the relaxation times for the binding of the 20-mer, dεA(pεA)$_{19}$, to the DnaB helicase in buffer T2 (pH 8.1, 100 mM NaCl, 1 mM AMP-PNP, 10 °C) upon the total concentration of dεA(pεA)$_{19}$. The continuous lines are non-linear least-squares fits according to the three-step sequential mechanism, defined by equation (1), with the rate constants: $k_1 = 3.4 \times 10^4$ M^{-1} s^{-1}, $k_{-1} = 0.018$ s^{-1}, $k_2 = 0.021$ s^{-1}, $k_{-2} = 0.01$ s^{-1}, $k_3 = 0.004$ s^{-1}, and $k_{-3} = 0.0012$ s^{-1} (see the text for details); (a) $1/\tau_1$, (b) $1/\tau_2$, (c) $1/\tau_3$. The error bars are standard deviations obtained from three or four independent experiments.

dependence becomes linear at the high 20-mer concentrations, although there is a non-linear phase at the low [dεA(pεA)$_{19}$] concentration. Such behavior is typical for the relaxation time characterizing the bimolecular binding step (see Figure 1(a)). On the other hand, both $1/\tau_2$ and $1/\tau_3$ show hyperbolic dependence upon [dεA(pεA)$_{19}$] and reach plateaus at high ssDNA concentrations. The minimum mechanism that can account for the observed dependence of the relaxation times upon the dεA(pεA)$_{19}$ concentration is a three-step, sequential binding process in which bimolecular association is followed by two isomerization steps as described by Scheme 1:

$$\text{Helicase} + \text{ssDNA} \underset{k_{-1}}{\overset{k_1}{\leftrightarrow}} (\text{H}-\text{ssDNA})_1 \underset{k_{-2}}{\overset{k_2}{\leftrightarrow}} (\text{H}-\text{ssDNA})_2 \underset{k_{-3}}{\overset{k_3}{\leftrightarrow}} (\text{H}-\text{ssDNA})_3$$

Scheme 1.

The continuous lines in Figure 4 are computer fits of the relaxation times according to the above mechanism. First, the analysis was performed by numerical, non-linear least-squares fitting of the individual relaxation times, then, the values of the rate constants were refined by global fitting that simultaneously includes all relaxation times. The obtained rate constants for the mechanism defined by Scheme 1 are: $k_1 = 3.4(\pm 0.6) \times 10^4$ M^{-1} s^{-1}, $k_{-1} = 0.018(\pm 0.005)$ s^{-1}, $k_2 = 0.021(\pm 0.005)$ s^{-1}, $k_{-2} = 0.01(\pm 0.003)$ s^{-1}, $k_3 = 0.004(\pm 0.001)$ s^{-1}, and $k_{-3} = 0.0012(\pm 0.0005)$ s^{-1} (Table 1).

The equilibrium association binding constants for each step in Scheme 1 are: $K_1 = k_1/k_{-1}$, $K_2 = k_2/k_{-2}$, and $K_3 = k_3/k_{-3}$. Introducing the values of the rate constants provides $K_1 = 1.9(\pm 0.6) \times 10^6$ M^{-1}, $K_2 = 2.1(\pm 1)$, and $K_3 = 3.3(\pm 1)$. Thus, the first step has a predominant contribution to the free energy of ssDNA binding, although the next two steps also increase the affinity. The overall binding constant, K_{20}, is related to the partial equilibrium steps by:

$$K_{20} = K_1(1 + K_1K_2 + K_1K_2K_3) \qquad (22)$$

The value of $K_{20} = 3(\pm 1) \times 10^7$ M^{-1} has been obtained independently in the same solution conditions by the equilibrium fluorescence titration method (Jezewska *et al.*, 1996; Jezewska & Bujalowski, 1996a). Introducing the values of equilibrium constants for partial equilibrium steps into equation (22) gives $K_{20} = 1.9(\pm 0.7) \times 10^7$ M^{-1}. Within experimental accuracy, this value of the overall binding constant is in excellent agreement with the K_{20}, determined by equilibrium titrations (Table 1).

Individual amplitudes of relaxation steps in the 20-mer, dεA(pεA)$_{19}$, binding to the DnaB hexamer

The dependence of the individual amplitudes, A_1, A_2, and A_3, of all three relaxation steps upon the dεA(pεA)$_{19}$ concentration, is shown in Figure 5. The individual amplitudes are expressed as fractions of the total amplitude, $A_i/\Sigma A_i$. At a low DNA concentration, only the amplitudes A_2 and A_3 of the second and third relaxation steps have a detectable contribution to A_{tot}. The amplitude A_2 goes through a maximum, while A_3 decreases steadily with the [dεA(pεA)$_{19}$]. As the concentration of the 20-mer increases, the amplitude of the first step, A_1, (bimolecular binding) increases and becomes a dominant relaxation effect.

Such behavior of the individual amplitudes is in full agreement with the proposed mechanism

Table 1. Kinetic, thermodynamic, and spectroscopic parameters characterizing the binding of the ssDNA 20-mer, dεA(pεA)$_{19}$, and the 10-mer, dεA(pεA)$_9$, to the *E. coli* DnaB helicase in buffer T2 (pH 8.1, 100 mM NaCl, 1 mM AMP-PNP, 10 °C)

Oligomer	k_1 (M^{-1} s^{-1})	k_{-1} (s^{-1})	k_2 (s^{-1})	k_{-2} (s^{-1})	k_3 (s^{-1})	k_{-3} (s^{-1})	K_1 (M^{-1})	K_2	K_3	Overall binding constant (M^{-1})	Overall binding constant[a] (M^{-1})	ΔF_2[b]	ΔF_3[b]	ΔF_4[b]
dεA(pεA)$_{19}$	3.4 (±0.6) × 10^4	0.018 (±0.005)	0.021 (±0.005)	0.01 (±0.003)	0.004 (±0.001)	0.0012 (±0.0005)	1.9 (±0.6) × 10^6	2.1 (±1)	3.3 (±1)	1.9 (±0.7) × 10^7	3 (±1) × 10^7	3.3 (±0.4)	4.1 (±0.4)	4.1 (±0.4)
dεA(pεA)$_9$	6.2 (±0.7) × 10^4	0.03 (±0.01)	0.06 (±0.01)	0.015 (±0.005)	0.006 (±0.002)	0.0045 (±0.002)	2.1 (±0.7) × 10^6	4 (±1.5)	1.3 (±0.5)	2.1 (±0.7) × 10^7	1.9 (±0.6) × 10^7	4.0 (±0.4)	5.0 (±0.5)	5.6 (±0.5)

[a] Determined in equilibrium fluorescence titrations (Jezewska & Bujalowski, 1996a; Jezewska *et al.*, 1998c).
[b] Values relative to the fluorescence, $\Delta F_1 = 1$ of the free 20-mer, dεA(pεA)$_{19}$, and the 10-mer, dεA(pεA)$_9$ (see the text for details).

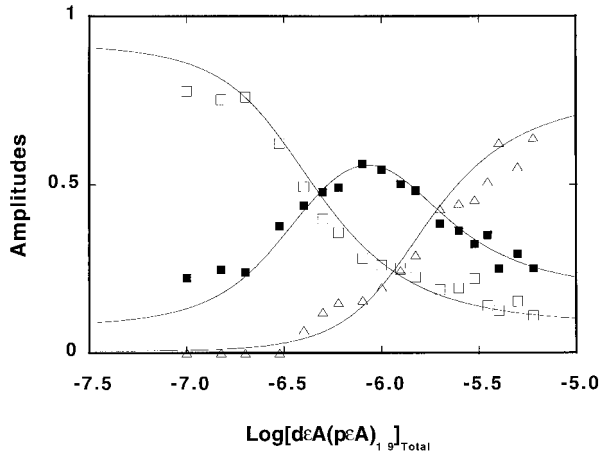

Figure 5. The dependence of the individual relaxation amplitudes for the binding of the 20-mer, dεA(pεA)$_{19}$, to the DnaB helicase in buffer T2 (pH 8.1, 100 mM NaCl, 1 mM AMP-PNP, 10 °C) upon the logarithm of the total concentration of dεA(pεA)$_{19}$. The continuous lines are non-linear least-squares fits according to the three-step sequential mechanism, defined by equation (1), with the relative fluorescence intensities $\Delta F_1 = 1$, $\Delta F_2 = 3.3$, $\Delta F_3 = 4.1$, and $\Delta F_4 = 4.1$. The maximum fractional fluorescence increase of the nucleic acid is taken from the equilibrium fluorescence titration, in the same solution conditions, as $\Delta F_{max} = 3.1$ (Jezewska *et al.*, 1996). The rate constants are the same as obtained from the relaxation time analysis (Table 1); A_1 (△), A_2 (■), A_3 (□).

(Scheme 1) deduced from the relaxation time analysis (see also Figure 3). However, the amplitude analysis, using the matrix projection operator technique, also allows us to determine the molar fluorescence intensities characterizing each intermediate of the reaction, i.e. to assess the conformational state of the protein-nucleic acid complex in each intermediate. This determination is facilitated by the fact that the maximum, fractional increase of the nucleic acid fluorescence is known from the equilibrium titrations, $\Delta F_{max} = 3.1$ (Bujalowski & Jezewska, 1995; Jezewska & Bujalowski, 1996a). Moreover, ΔF_{max} can be analytically expressed as:

$$\Delta F_{max} = \frac{\Delta F_2}{1 + K_2 + K_2K_3} + \frac{K_2\Delta F_3}{1 + K_2 + K_2K_3} + \frac{K_2K_3\Delta F_4}{1 + K_2 + K_2K_3} \quad (23)$$

where ΔF_2, ΔF_3, and ΔF_4 are molar fluorescence intensities of each intermediate in the association reaction of the DnaB helicase with the 20-mer, relative to the fluorescence of the free nucleic acid, ΔF_1. Notice, these fluorescence parameters are relative fluorescence intensities, but not fractional intensities, with respect to the free nucleic acid fluorescence. Equation (23) provides an additional relationship among the fluorescence parameters, with the value of ΔF_{max} playing the role of a scaling factor. The continuous lines in Figure 5 are computer fits of the experimentally determined fractional individual amplitudes of the reaction using equations (19)-(21). The applied fitting procedure was similar to that used for the relaxation times described above. First, non-linear least-squares fitting was performed with the individual amplitudes using the same rate constants as those obtained from the examination of the relaxation times, or allowing the rate constants to float between ±10 % of the values determined in the relaxation time analysis. Both approaches provide similar values of the relative fluorescence intensities. Finally, global fitting, with the simultaneous analysis of all three individual amplitudes, refined the obtained parameters. The fluorescence of the free dεA(pεA)$_{19}$ was taken as $\Delta F_1 = 1$. The results indicate that the largest fluorescence change, as compared to the free 20-mer, occurs in the first binding step, i.e. in the formation of the (H-ssDNA)$_1$. Upon formation of this complex, the fluorescence of the 20-mer increases by a factor of 3.3 ($\Delta F_2 = 3.3 \pm 0.4$) as compared to the free DNA. Conformational transition to the (H-ssDNA)$_2$ induces only an ~30 % additional increase of the 20-mer fluorescence over ΔF_1 ($\Delta F_3 = 4.1(\pm 0.4)$), while the transition to the (H-ssDNA)$_3$ is not accompanied by an additional fluorescence increase over ΔF_3 ($\Delta F_4 = 4.1(\pm 0.4)$) (see Discussion).

Effect of the protein concentration on the measured relaxation times of the dεA(pεA)$_{19}$-DnaB helicase association

The stability of the DnaB hexamer is an important factor in the examination of the helicase-ssDNA complex formation. Any dissociation of the hexamer into lower oligomers would obscure the kinetic processes and the possibility of quantitatively interpreting it, unless the kinetics of such dissociation and its effect on the dynamics of the DNA binding is also examined. On the other hand, dissociation of the hexamer could be a part of the binding mechanism. Figure 6(a)-(c) shows the determined relaxation times, as a function of the [DnaB] (hexamer), over an order of magnitude change of the protein concentration. The data clearly show that, within experimental accuracy, all three relaxation times are independent of the helicase concentration, indicating that the observed kinetics are not affected by the protein-protein interactions. Also, the lack of a protein concentration on the observed kinetic process indicates that the DnaB protein hexamer does not dissociate prior to binding the ssDNA, but rather the entry of the ssDNA into the cross-channel of the hexamer occurs through a local opening of the hexamer (see Discussion).

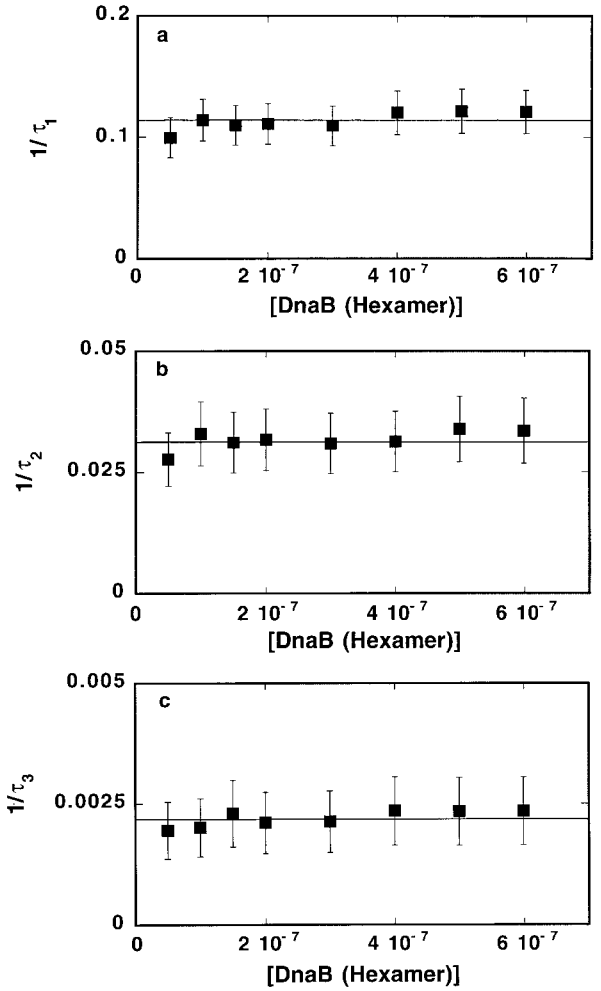

Figure 6. The dependence of the reciprocal relaxation times of the dεA(pεA)$_{19}$-DnaB helicase system upon the enzyme concentration (hexamer) in buffer T2 (pH 8.1, 100 mM NaCl, 1 mM AMP-PNP, 10°C); (a) $1/\tau_1$, (b) $1/\tau_2$, (c) $1/\tau_3$. The error bars are standard deviation obtained from three or four independent experiments.

Kinetics of the 10-mer, dεA(pεA)$_9$, binding to the DnaB helicase

The total ssDNA-binding site of the DnaB helicase is built of two subsites, a strong and a weak ssDNA-binding region, which occlude a similar ~10 nucleotide residues of the ssDNA (Jezewska *et al.*, 1998c). The question to answer is: how does the mechanism of the association of the 20-mer, which encompasses the entire total binding site of the DnaB helicase, reflect the interactions of the enzyme with the partial ligand that binds exclusively to the strong ssDNA binding subsite?

As in the case of the 20-mer, the stopped-flow experiments have been performed under pseudo-first-order conditions by mixing the DnaB with a large excess of the 10-mer. The stopped-flow kinetic trace of the dεA(pεA)$_9$ fluorescence, after mixing 5×10^{-6} M oligomer 10-mer with 1.5×10^{-7} M hexamer DnaB helicase (final concentrations) in buffer T2 (pH 8.1, 100 mM NaCl, 1 mM AMP-PNP, 10°C), is shown in Figure 7. The curve has been recorded in two time bases, 10 and 1000 seconds. As shown by the included deviations from the fit, the observed kinetic curve is adequately described by a three-exponential function, but not by a two-exponential function. Thus, similar to the 20-mer, the association of the ssDNA 10-mer with the strong ssDNA-binding subsite of the DnaB helicase includes at least three steps.

The reciprocal relaxation times, $1/\tau_1$, $1/\tau_2$, and $1/\tau_3$, characterizing the three binding processes, as a function of the total dεA(pεA)$_9$ concentration, are shown in Figure 8(a)-(c). The largest reciprocol relaxation time, $1/\tau_1$, increases with [dεA(pεA)$_9$] as expected for the relaxation time characterizing the bimolecular binding step (see Figures 2 and 4). Both $1/\tau_2$ and $1/\tau_3$ show hyperbolic dependence upon the [dεA(pεA)$_9$] and reach plateaus at high ssDNA concentrations. Therefore, the association of the 10-mer with the strong ssDNA-binding subsite can be described by the same mechanism as determined for the 20-mer, in which the bimolecular association is followed by two conformational transitions of the formed complex (Scheme 1).

The continuous lines in Figure 8(a)-(c) are computer fits of the relaxation times according to the three-step mechanism (Scheme 1), which provide the following rate constants: $k_1 = 6.2(\pm 0.7) \times 10^4$ M^{-1} s^{-1}, $k_{-1} = 0.03(\pm 0.01)$ s^{-1}, $k_2 = 0.06(\pm 0.01)$ s^{-1}, $k_{-2} = 0.015(\pm 0.005)$ s^{-1}, $k_3 = 0.006(\pm 0.002)$ s^{-1}, and $k_{-3} = 0.0045(\pm 0.002)$ s^{-1}. The data show that, although the binding of the mechanism of the 10-mer, dεA(pεA)$_9$, is the same as that determined for the larger ligand, dεA(pεA)$_{19}$, the values of all rate constants are higher (Table 1) (see Discussion).

Analysis of the amplitudes of the kinetic process of dεA(pεA)$_9$, binding to the DnaB helicase

The dependence of the total, A_{tot} and individual amplitudes, A_1, A_2, and A_3 of all three relaxation steps upon the logarithm of the total dεA(pεA)$_9$ concentration is shown in Figure 9. The individual amplitudes are expressed as a fraction of the total amplitude, while the total amplitude is normalized to 1 at saturating concentrations of the nucleic acid. Molar fluorescence intensities characterizing each intermediate of the reaction, relative to the molar fluorescence of the free 10-mer, have been obtained using the matrix projection operator technique, described above, and the relationship defined by equation (23). The maximum, fractional increase of the 10-mer fluorescence, upon saturation with the DnaB helicase, is known from the equilibrium titrations with the value used in these calculations, $\Delta F_{max} = 4.2$ (Jezewska *et al.*, 1998c). The continuous lines in Figure 9 are non-linear least-squares fits of the experimentally determined fractional individual amplitudes of the reaction, using equations (18)-(21) and equation (23), with

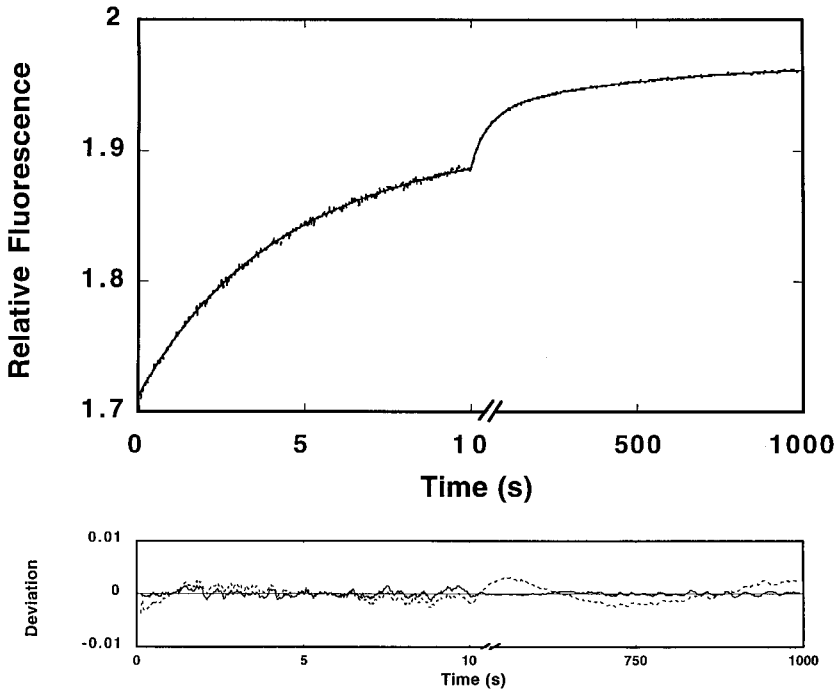

Figure 7. The top panel is the fluorescence stopped-flow kinetic trace, recorded in two time bases, ten seconds and 1000 seconds, after mixing the DnaB with the 10-mer, dεA(pεA)$_9$ in buffer T2 (pH 8.1, 100 NaCl, 1 mM AMP-PNP, 10 °C) ($\lambda_{ex} = 320$ nm, $\lambda_{em} > 400$ nm). The final concentrations of the helicase and the 10-mer are 1.5×10^{-7} M (hexamer) and 5×10^{-6} M (oligomer), respectively. The continuous line is the three-exponential, non-linear least-squares fit of the experimental curve using equation (26). The lower panel shows the deviation of the experimental curve from the fit using two-exponential (broken line) and three-exponential (continuous line) functions (equation (26)), respectively.

the fluorescence of the free dεA(pεA)$_9$ taken as 1. The fitting procedure is the same as that applied for the 20-mer.

All relative fluorescence increases are larger than obtained for the 20-mer because the maximum increase of the 10-mer fluorescence is larger upon saturation with the helicase (Table 1; Jezewska *et al.*, 1998c). However, similar to the 20-mer, the major fluorescence change occurs in the formation of the (H-ssDNA)$_1$ with $\Delta F_1 = 4.0(\pm 0.4)$. Conformational transition to the (H-ssDNA)$_2$ induces only an ~25% additional increase of the 10-mer fluorescence over the (H-ssDNA)$_1$ with $\Delta F_2 = 5.0(\pm 0.5)$. Formation of the (H-ssDNA)$_3$ is accompanied by an additional ~10% fluorescence change with $\Delta F_3 = 5.6(\pm 0.5)$.

Stopped-flow kinetic studies of the binding of dεA(pεA)$_4$(pT)$_{15}$ and dεA(pεA)$_4$(pA)$_{15}$ oligomers to the DnaB hexamer

In solution conditions, similar to these applied in our studies, adenosine homooligomers have an ordered structure with significant stacking interactions between bases (Porschke, 1973; Baker *et al.*, 1978; Saenger, 1984). On the other hand, thymine oligomers form disordered structures with very limited base-base stacking interactions (Saenger, 1984). To address the role of the nucleic acid structure in observed kinetics of the ssDNA binding to the DnaB helicase, we performed experiments with two 20-mers, dεA(pεA)$_4$(pT)$_{15}$ and dεA(pεA)$_4$(pA)$_{15}$. Each oligomer has a short stretch of five etheno-adenosine residues at its 5′ end that provide the signal to monitor the interactions.

Stopped-flow kinetic traces for both dεA(pεA)$_4$(pT)$_{15}$ and dεA(pεA)$_4$(pA)$_{15}$ are adequately described by a three-exponential function, although the observed signal is much weaker, due to the much lower fluorescence of both oligomers, resulting from the low content of the fluorescent etheno-adenosine residues. Thus, similar to the dεA(pεA)$_{19}$ and dεA(pεA)$_9$, the association of dεA(pεA)$_4$(pT)$_{15}$ and dεA(pεA)$_4$(pA)$_{15}$ with the DnaB helicase includes at least three steps. The reciprocal relaxation times, $1/\tau_1$, $1/\tau_2$, and $1/\tau_3$, as a function of the total dεA(pεA)$_4$(pT)$_{15}$ concentration in buffer T2 (pH 8.1, 100 mM NaCl, 1 mM AMP-PNP, 10 °C), are shown in Figure 10(a)-(c). The largest reciprocal relaxation time, $1/\tau_1$, increases with the [dεA(pεA)$_4$(pT)$_{15}$], as expected for the relaxation time characterizing the bimolecular binding step, while both $1/\tau_2$ and $1/\tau_3$ reach plateaus at high oligomer concentrations. Thus, the association of the dεA(pεA)$_4$(pT)$_{15}$ with the helicase can be described by the same mechanism as that determined for the dεA(pεA)$_{19}$ and dεA(pεA)$_9$ in which the bimolecular association is followed by two conformational transitions of the formed complex (Scheme 1). Binding of oligomers with the

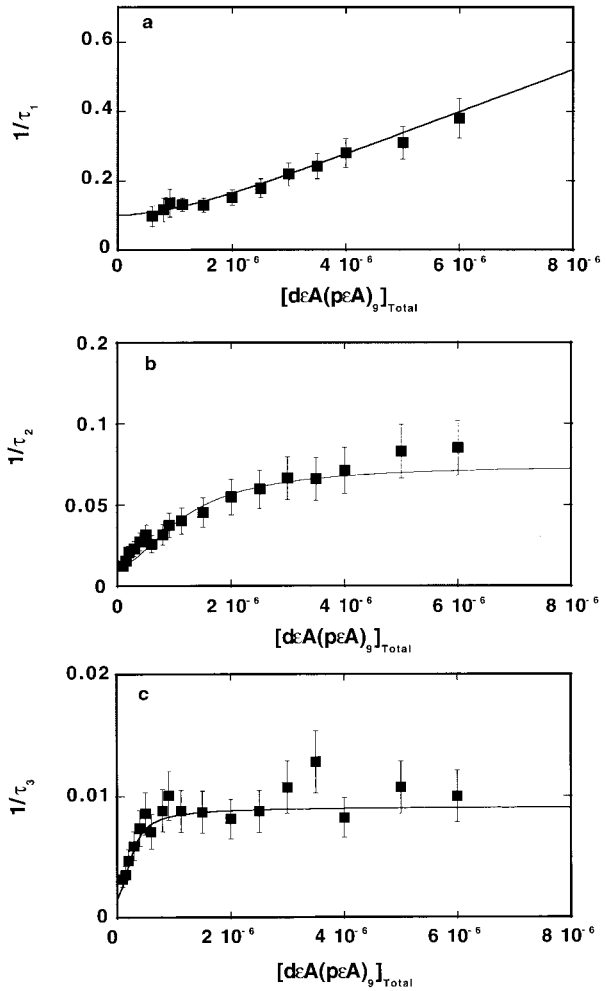

Figure 8. The dependence of the reciprocal of the relaxation times for the binding of the 10-mer, dεA(pεA)$_9$, to the DnaB helicase in buffer T2 (pH 8.1, 100 mM NaCl, 1 mM AMP-PNP, 10 °C) upon the total concentration of dεA(pεA)$_9$. The continuous lines are non-linear least-squares fits according to the three-step sequential mechanism, defined by equation (1), with the rate constants: $k_1 = 6.2 \times 10^4$ M^{-1} s^{-1}, $k_{-1} = 0.03$ s^{-1}, $k_2 = 0.06$ s^{-1}, $k_{-2} = 0.015$ s^{-1}, $k_3 = 0.006$ s^{-1}, and $k_{-3} = 0.0045$ s^{-1}, (a) $1/\tau_1$, (b) $1/\tau_2$, (c) $1/\tau_3$. The error bars are standard deviations obtained from three or four independent experiments.

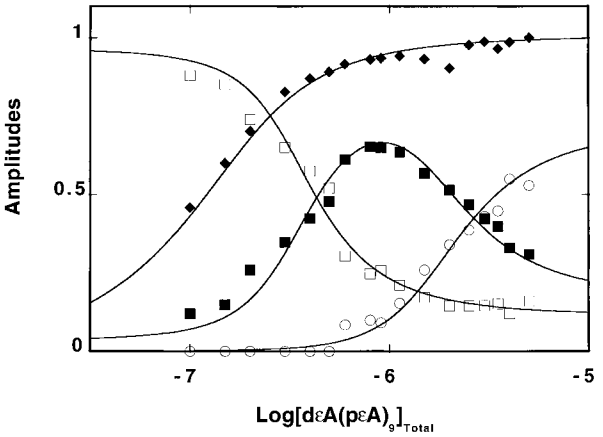

Figure 9. The dependence of the individual and total relaxation amplitudes for the binding of the 10-mer, dεA(pεA)$_9$, to the DnaB helicase in buffer T2 (pH 8.1, 100 mM NaCl, 1 mM AMP-PNP, 10 °C) upon the logarithm of the total concentration of dεA(pεA)$_{19}$. The continuous lines are non-linear least-squares fits according to the three-step sequential mechanism, defined by equation (1), with the relative fluorescence intensities $\Delta F_1 = 1$, $\Delta F_2 = 4.0$, $\Delta F_3 = 5.0$, and $\Delta F_4 = 5.6$. The maximum fluorescence increase of the nucleic acid upon saturation with the helicase has been determined in equilibrium fluorescence titrations, in the same solution conditions, as $\Delta F_{max} = 4.2$ (Jezewska *et al.*, 1998c). The rate constants are the same as obtained from the relaxation time analysis (Table 1); A_{tot} (◆), A_1 (○), A_2 (■), A_3 (□).

stretch of five etheno-adenosine residues located at their 3′ end is characterized by the same kinetic mechanism (data not shown). The continuous lines in Figure 10 are computer fits of the relaxation times according to the three-step mechanism (Scheme 1), which provide the following rate constants: $k_1 = 3.1(\pm 0.6) \times 10^4$ M^{-1} s^{-1}, $k_{-1} = 0.025(\pm 0.007)$ s^{-1}, $k_2 = 0.035(\pm 0.01)$ s^{-1}, $k_{-2} = 0.012(\pm 0.005)$ s^{-1}, $k_3 = 0.0021(\pm 0.001)$ s^{-1}, and $k_{-3} = 0.001(\pm 0.0005)$ s^{-1}. Binding of the dεA(pεA)$_4$(pA)$_{15}$ is characterized by virtually the same kinetic parameters, showing that the difference in the ssDNA structure, the extent of stacking interactions, and the type of base has little effect on the kinetics of the 20-mer binding (Table 2; see Discussion).

The dependence of the individual amplitudes, A_1, A_2, and A_3, of all three relaxation steps upon the logarithm of the total dεA(pεA)$_4$(pT)$_{15}$ concentration is shown in Figure 11. The individual amplitudes are expressed as a fraction of the total amplitude. Molar fluorescence intensities characterizing each intermediate of the reaction, relative to the molar fluorescence of the free nucleic acid, have been obtained using the matrix projection operator technique, described above. The continuous lines in Figure 11 are computer fits of the experimentally determined fractional individual amplitudes of the reaction using equations (18)-(21) and equation (23) with the fluorescence of the free 20-mer taken as 1. All relative fluorescence increases are significantly lower than those obtained for the dεA(pεA)$_{19}$ and dεA(pεA)$_9$ (Table 1). This is because the maximum increase of fluorescence of both dεA(pεA)$_4$(pT)$_{15}$ and dεA(pεA)$_4$(pA)$_{15}$ upon saturation with the DnaB protein is lower than in the case of homoetheno-adenosine oligomers (Table 2; Figure 11). However, similar to dεA(pεA)$_{19}$ and dεA(pεA)$_9$, the major fluorescence change of dεA(pεA)$_4$(pT)$_{15}$ and dεA(pεA)$_4$(pA)$_{15}$ occurs in the formation of the (H-ssDNA)$_1$ (Table 2).

Table 2. Kinetic, thermodynamic, and spectroscopic parameters characterizing the binding of the ssDNA 20-mers, dεA(pεA)$_4$(pT)$_{15}$ and dεA(pεA)$_4$(pA)$_{15}$, to the *E. coli* DnaB helicase in buffer T2 (pH 8.1, 100 mM NaCl, 1 mM AMP-PNP, 10 °C)

Oligomer	k_1 (M^{-1} s^{-1})	k_{-1} (s^{-1})	k_2 (s^{-1})	k_{-2} (s^{-1})	k_3 (s^{-1})	k_{-3} (s^{-1})	K_1 (M^{-1})	K_2	K_3	Overall binding constant (M^{-1})	Overall binding constant[a] (M^{-1})	ΔF_2[b]	ΔF_3[b]	ΔF_4[b]
dεA(pεA)$_4$	3.1	0.025	0.035	0.012	0.0021	0.001	1.2	2.9	1.8	1.2	1.1	2.3	2.7	3
(pT)$_{15}$	(±0.6) × 10^4	(±0.007)	(±0.01)	(±0.005)	(±0.001)	(±0.0005)	(±0.4) × 10^6	(±0.7)	(±0.6)	(±0.4) × 10^7	(±0.3) × 10^7	(±0.3)	(±0.4)	(±0.4)
dεA(pεA)$_4$	3.1	0.025	0.04	0.012	0.0024	0.0013	1.2	3.3	1.6	1.3	1.1	2.3	2.7	3
(pA)$_{15}$	(±0.6) × 10^4	(±0.007)	(±0.01)	(±0.005)	(±0.001)	(±0.0005)	(±0.5) × 10^6	(±1)	(±0.5)	(±0.5) × 10^7	(±0.3) × 10^7	(±0.3)	(±0.4)	(±0.5)

[a] Determined in equilibrium fluorescence titrations.
[b] Values relative to the fluorescence, $\Delta F_1 = 1$ of the free 20-mers, dεA(pεA)$_4$(pT)$_{15}$ and dεA(pεA)$_4$(pεA)$_{15}$ (see the text for details).

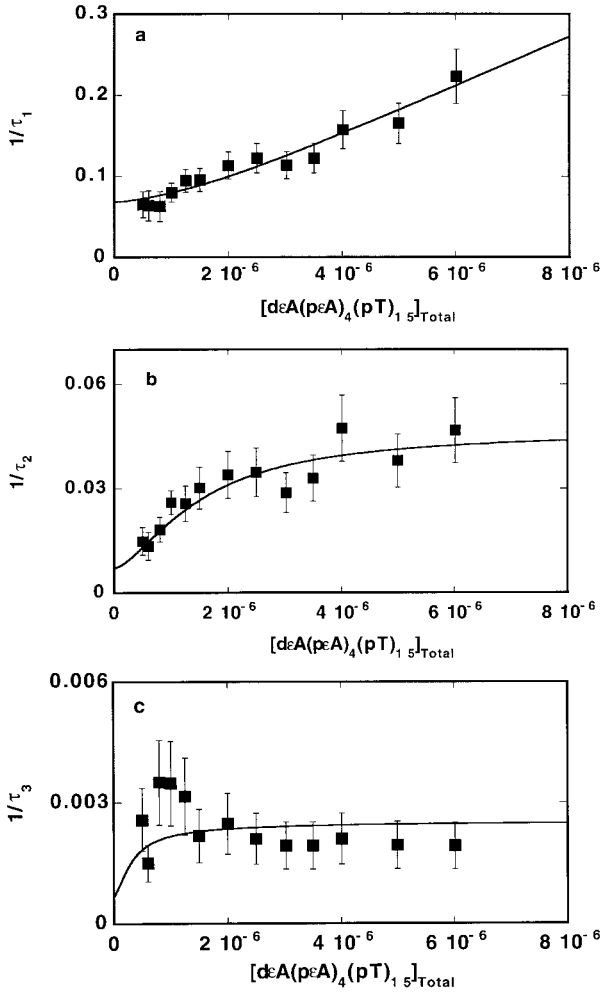

Figure 10. The dependence of the reciprocal of the relaxation times for the binding of the 20-mer, $d\varepsilon A(p\varepsilon A)_4(pT)_{15}$, to the DnaB helicase in buffer T2 (pH 8.1, 100 mM NaCl, 1 mM AMP-PNP, 10 °C) upon the total concentration of $d\varepsilon A(p\varepsilon A)_4(pT)_{15}$. The continuous lines are non-linear least-squares fits according to the three-step sequential mechanism, defined by equation (1), with the rate constants: $k_1 = 3.1 \times 10^4$ M^{-1} s^{-1}; $k_{-1} = 0.025$ s^{-1}, $k_2 = 0.035$ s^{-1}, $k_{-2} = 0.012$ s^{-1}, $k_3 = 0.0021$ s^{-1}, and $k_{-3} = 0.001$ s^{-1}; (a) $1/\tau_1$, (b) $1/\tau_2$, (c) $1/\tau_3$. The error bars are standard deviations obtained from three or four independent experiments.

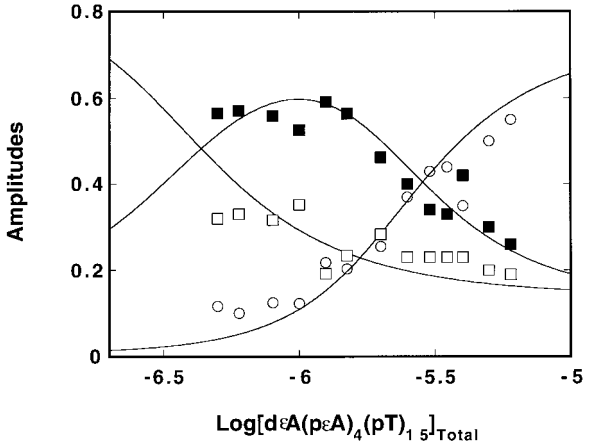

Figure 11. The dependence of the individual relaxation amplitudes for the binding of the 20-mer, $d\varepsilon A(p\varepsilon A)_4(pT)_{15}$, to the DnaB helicase in buffer T2 (pH 8.1, 100 mM NaCl, 1 mM AMP-PNP, 10 °C) upon the logarithm of the total concentration of $d\varepsilon A(p\varepsilon A)_4(pT)_{15}$. The continuous lines are non-linear least-squares fits according to the three-step sequential mechanism, defined by equation (1), with the relative fluorescence intensities $\Delta F_1 = 1$, $\Delta F_2 = 2.3$, $\Delta F_3 = 2.7$, and $\Delta F_4 = 3$. The maximum fluorescence increase of the nucleic acid upon saturation with the helicase has been determined in equilibrium fluorescence titrations, in the same solution conditions, as $\Delta F_{max} = 1.8$ (Table 2). Rate constants are the same as obtained from the relaxation time analysis (Table 2); A_1 (○), A_2 (■), A_3 (□).

Discussion

Elucidation of the energetics and dynamics aspects of the helicase interactions with its DNA substrates is one of the major prerequisites for understanding the enzyme activity at the molecular level (Lohman & Bjorson, 1996). In order to determine the mechanism of the ssDNA recognition by the DnaB helicase, we have undertaken stopped-flow kinetic studies of the enzyme-ssDNA complexes. The site-size of the *E. coli* DnaB hexameric helicase, in the complex with the ssDNA, is 20(±3) nucleotides per hexamer. Moreover, the hexamer binds a single molecule of the 20-mer that encompasses the entire total binding site of the enzyme. To directly address the interactions of the helicase with the nucleic acid within the binding site-size, without any interference of the possible protein-protein interactions, the stopped-flow experiments have been performed with 20-mer and 10-mer ssDNA oligomers. We previously determined that binding of the DnaB helicase to ssDNA oligomers is not affected by any detectable ''end effects'' (Jezewska *et al.*, 1996).

The DnaB helicase acquires strong affinity toward ssDNA only in the presence of ATP or ATP non-hydrolyzable analogs, e.g. AMP-PNP (Arai & Kornberg, 1981; Bujalowski & Jezewska, 1995; Jezewska & Bujalowski, 1996a; Jezewska *et al.*, 1996). However, as we pointed out before, the DnaB helicase is a potent ATPase even in the absence of the ssDNA (Bujalowski & Klonowska, 1993). Such strong ATPase activity would make any quantitative analysis of the enzyme binding to the ssDNA in the presence of ATP very difficult because of the multitude of different enzyme forms in solution whose concentrations change with time and whose interactions with the ssDNA can be very different. Therefore, the experiments reported here have been performed with a high ssDNA affinity form of the DnaB helicase, in the presence of a saturating concentration of the ATP non-hydrolyzable analog, AMP-PNP.

In our approach, we utilized the fact that the binding of the ssDNA containing the fluorescent etheno-derivative of adenosine to the DnaB helicase is accompanied by a strong nucleic acid fluorescence increase (Bujalowski & Jezewska, 1995; Jezewska & Bujalowski, 1996a; Jezewska *et al*., 1996, 1997). Such a large signal change upon forming a complex with the protein provides the necessary resolutions required to quantitatively assess the complex mechanism of ligand-macromolecule interactions. This is particularly important when the amplitudes of some relaxation processes are small and when there are large differences among the relaxation times.

Application of matrix projection operator technique to study stopped-flow kinetics

Complex relaxation kinetics are usually studied either by purely numerical methods or by using approximate formulas, justified by the properties of the studied system, for relaxation times and amplitudes (Bernasconi, 1976). Purely numerical methods are very powerful, but require sophisticated software and provide limited insight into the physical aspects of the studied mechanism, particularly, the nature and structure of the intermediates. On the other hand, approximate formulas, important for intuitive understanding, can be applied only in stringent conditions, not always fulfilled by the system, and can often miss some characteristics of the studied system, as we discussed above. The matrix projection operator technique, as described here, offers an experimenter the possibility of limiting the numerical analysis to finding only the eigenvalues of the coefficient matrix that are directly related to the relaxation times of the kinetic system. Once the eigenvalues are determined, the amplitudes of each resolved step of the reaction can be explicitly expressed in terms of the rate constants, relaxation times (eigenvalues), and spectroscopic properties of each intermediate by expanding the solution matrix using eigenvalues and corresponding projection operators. The approach provides closed-form expressions for the amplitudes of the complex, multistep kinetic mechanism (equations (18)-(21)). In the case of spectroscopic kinetic studies, as described here, analysis of the experimentally obtained amplitudes enables the determination of spectroscopic properties of all identified intermediates.

Multiple-step kinetic mechanism of the ssDNA 20-mer binding to the DnaB helicase

The results obtained in this work indicate that the mechanism of the ssDNA 20-mer, $d\varepsilon A(p\varepsilon A)_{19}$, binding to the DnaB helicase in the presence of the ATP non-hydrolyzable analog, AMP-PNP, is a minimum three-step, sequential process described by Scheme 1. The bimolecular association is followed by two isomerization processes. Thus, the enzyme-ssDNA complex undergoes at least two conformational transitions following the initial complex formation. The kinetic evidence of the conformational transition of the helicase-ssDNA complex following the binding, presented here, corroborates well with our previous results obtained using analytical ultracentrifugation (Jezewska & Bujalowski, 1996b). Association of the DnaB helicase with the ssDNA 20-mer is accompanied by a change of the enzyme sedimentation coefficient larger than expected from the increased molecular mass of the complex. However, it should be noticed that the value of the bimolecular association rate constant $k_1 = 3.4(\pm 0.6) \times 10^4$ M^{-1} s^{-1} is dramatically lower than expected for the diffusion-controlled reaction (Berry *et al*., 1980; Moore & Pearson, 1981). The intrinsic association rate constant could be even lower, because the six subunits of the DnaB hexamer are chemically identical, i.e. there could be six entry sites for the ssDNA. Thus, the determined association rate constant may contain a statistical factor as high as 6.

In chemical bimolecular reactions in solution, formation of a collision/encounter complex, a process that is controlled by diffusion of the reactants (Berry *et al*., 1980; Moore & Pearson, 1981), precedes formation of the product. Theoretical values of the maximum rate constant for the diffusion-controlled association can be estimated using the Smoluchowski equation (Moore & Pearson, 1981):

$$k_D = \frac{4\pi N_A (D_P + D_D)(r_P + r_D)}{1000} \qquad (24)$$

where N_A is Avogadro's number, D_P and D_D are diffusion coefficients of the protein and the nucleic acid, respectively, and r_P and r_D are their interaction radii. The diffusion coefficient of the DnaB helicase hexamer, corrected to our buffer conditions (buffer T2 (pH 8.1, 100 mM NaCl, 10 °C), $D_P = 2.8(\pm 0.3) \times 10^{-7}$ cm^2/second) has been determined using the dynamic light-scattering technique (unpublished results). The diffusion coefficient of the ssDNA 20-mer can be estimated from the Svedberg equation (Tanford, 1961):

$$D_D = \frac{sRT}{M_{20}(1 - \bar{\vartheta}\rho)} \qquad (25)$$

where s and M_{20} are the sedimentation coefficient and molecular mass of the 20-mer, R is the gas constant, T is the temperature (Kelvin), $\bar{\vartheta}$ is the ssDNA specific volume, and ρ is the solvent density. Using the analytical ultracentrifugation technique, we determined the sedimentation coefficient of the 20-mer $s_{20,w} = 1.4(\pm 0.12)$ S. Using this value of s and $M_{20} \approx 6400$ g/mol, $\bar{\vartheta} = 0.505$ ml/g, $\rho = 1$ g/ml, one obtains $D_D = 1.1 \times 10^{-6}$ cm^2/second (Bujalowski *et al*., 1986b). Correcting this value to our buffer conditions, one obtains $D_D = 6.1 \times 10^{-7}$ cm^2/second (Tanford, 1961). The interacting radii have been taken as equal to the approximate size of the 20-mer $r_D = r_P \sim 68$ Å.

With these values, the diffusion-controlled association rate constant is $k_D \sim 8.9 \times 10^9$ M^{-1} s^{-1}. Smaller interaction radii and/or orientation factors could lower this value to k_D $\sim 10^7$-10^8 M^{-1} s^{-1}, which is similar to the values observed for some very fast formations of the single-stranded nucleic acid oligomers-protein complexes (Mulsch *et al.*, 1981). In spite of the approximate nature of these estimates, the determined bimolecular rate constant k_1 is about three to six orders of magnitude lower than the k_D predicted by the diffusion-controlled collision, indicating that the bimolecular association step contains an additional, conformational transition of the helicase-ssDNA complex. This conclusion is also evident from the amplitude analysis, which shows that the largest increase of the nucleic acid fluorescence in the complex with the DnaB helicase (most probably the largest conformational change) occurs in the formation of the $(H\text{-ssDNA})_1$ (see below). Such dramatic conformational changes cannot take place in a collision complex, because then it would not be a collision complex (Berry *et al.*, 1980; Moore & Pearson, 1981). Therefore, Scheme 1 should be enlarged by an extra step following the collision complex, E, as described by Scheme 2:

$$\text{Helicase} + \text{ssDNA} \overset{k_D}{\underset{k_{-D}}{\leftrightarrow}} \text{E} \overset{k_1'}{\underset{k_{-1}'}{\leftrightarrow}} (\text{H-ssDNA})_1 \overset{k_2}{\underset{k_{-2}}{\leftrightarrow}} (\text{H-ssDNA})_2 \overset{k_3}{\underset{k_{-3}}{\leftrightarrow}} (\text{H-ssDNA})_3$$

Scheme 2.

where k_D and k_{-D} are rate constants for the formation and dissociation of the collision complex, and k_1' and k_{-1}' are the rate constants for the transition from the collision complex to the $(H\text{-ssDNA})_1$. The equilibrium constant for the first step is then $K_D = k_D/k_{-D}$. Because the formation of E is a very fast process and equilibrates before any significant transition to the $(H\text{-ssDNA})_1$ takes place, the observed, apparent bimolecular rate constant is $k_1 = K_D\, k_1'$. Inspection of Figure 3 shows that there is no amplitude lost in the dead-time of the instrument (~1.4 ms). The lack of any amplitude corresponding to the formation of the collision complex results from the fact that the process is very fast and there is no conformational transition accompanying its formation.

The estimate of the range of the values of k_1' can be obtained as follows. Notice that the dependence of the reciprocal relaxation time for the bimolecular process, $1/\tau_1$, is a linear function of the nucleic acid concentration at the highest concentrations examined ($\sim 6 \times 10^{-6}$ M). This shows that K_D is much lower than $\sim 2 \times 10^5$ M^{-1} (Bernasconi, 1976). Taking a conservative value of $K_D \sim 10^4$ M^{-1} gives $k_1' \sim 3.4$ s^{-1}. Thus, the data indicate that the collision complex E undergoes a transition to the $(H\text{-ssDNA})_1$, which has a forward rate constant of about two to three orders of magnitude larger than the forward rate constants for the subsequent formation of the $(H\text{-ssDNA})_2$ and $(H\text{-ssDNA})_3$.

Observed ssDNA fluorescence changes suggest that major conformational transition of the nucleic acid in the complex with the DnaB helicase occurs in the first binding step

The functional dependence of the individual amplitudes, A_1, A_2, and A_3, of the relaxation processes in the DnaB helicase association reaction with the ssDNA 20-mer fully support the sequential character of the binding mechanism (Figures 2 and 5). Moreover, the amplitude analysis indicates that the largest fluorescence increase accompanies the formation of the $(H\text{-ssDNA})_1$ complex. Notice, at the excitation wavelength applied ($\lambda_{ex} = 320$ nm), only the etheno-adenosine is excited. Thus, the observed fluorescence increase results from a nucleic acid quantum yield increase in the complex with the helicase, not through energy transfer processes. We previously determined that tryptophan residues of the DnaB protein are located far enough away from the ssDNA-binding site to eliminate any efficient energy transfer (Bujalowski & Klonowska, 1994a,b).

The fluorescence of εA is dramatically quenched (between eight- and tenfold) in the etheno-oligomers as compared to the free εAMP (Tolman *et al.*, 1974; Baker *et al.*, 1978). Stacking interactions among neighboring εA bases is similar to stacking interactions in unmodified adenosine polymers (Baker *et al.*, 1978). The quenching of the εA fluorescence has been modeled as a dynamic phenomenon in which the motion of the εA leads to quenching *via* intramolecular collision. Fluorescence of the etheno-derivative depends little on solvent conditions (Secrist *et al.*, 1972; Bujalowski & Klonowska, 1994b). In other words, changes of the fluorescence of the etheno-derivative ssDNA oligomers are induced predominantly through conformational changes of the nucleic acid. This is a particularly useful property of the etheno-derivatives. The observed strong fluorescence increase of the etheno-derivative ssDNA oligomers upon binding to the DnaB helicase indicates significantly restricted mobility and separation of the nucleic acid bases in the complex with the enzyme (Jezewska *et al.*, 1996). The largest fluorescence increase observed in the formation of the $(H\text{-ssDNA})_1$ strongly suggests that these dramatic changes of the nucleic acid conformation occur in the formation of this complex and are preserved in the $(H\text{-ssDNA})_2$ and $(H\text{-ssDNA})_3$. As we pointed out, a large conformational change accompanying the formation of the $(H\text{-ssDNA})_1$ argues against the possibility that this complex is the result of a simple collision or encounter.

Comparison between $d\varepsilon A(p\varepsilon A)_{19}$, $d\varepsilon A(p\varepsilon A)_4(pT)_{15}$, and $d\varepsilon A(p\varepsilon A)_4(pA)_{15}$ puts additional light on the nature of the $(H\text{-ssDNA})_1$ complex. All three 20-mers differ dramatically in the type of base, however, they bind with the same mechanism and their kinetic parameters are very similar, indicating that the dynamics of the ssDNA associ-

ation with the DnaB helicase is largely base-independent (Tables 1 and 2). These results corroborate our thermodynamic studies, which showed that the energetics of the 20-mer binding to the enzyme is base-independent (Jezewska *et al.*, 1996). Moreover, while $d\varepsilon A(p\varepsilon A)_{19}$ and $d\varepsilon A(p\varepsilon A)_4(pA)_{15}$ form ordered helical structures in solution, with strong stacking interactions between bases, $d\varepsilon A(p\varepsilon A)_4(pT)_{15}$ exists mostly in a disordered state, with very limited stacking interactions between the bases (Saenger, 1984). The very similar rate constants in all kinetic steps for all three 20-mers indicate that the structure of the free single-stranded nucleic acid in solution does not affect the dynamics of the ssDNA recognition by the DnaB helicase.

Conformational transitions of the single-stranded nucleic acid oligomers, particularly base stacking, are very fast processes that occur in the range of microseconds (Porschke, 1973, 1976, 1978). The fact that the transition from the collision complex E to the $(H\text{-ssDNA})_1$ is characterized by the rate constant in the range of $\sim 3\ s^{-1}$ indicates that this is not exclusively the change of the nucleic acid structure upon association, but rather a conformational transition of the enzyme-ssDNA complex. In other words, the observed dynamics of the formation of the $(H\text{-ssDNA})_1$ is an intrinsic property of the DnaB helicase, in response to the nucleic acid binding, and not simply an adjustment of the bound ssDNA to the structure of the enzyme binding site.

Strong ssDNA-binding subsite of the DnaB helicase is predominantly involved in ssDNA recognition by the enzyme

The total ssDNA-binding site of the DnaB helicase is built of two functionally and structurally different regions, strong and weak ssDNA-binding subsites that occlude about ten nucleotide residues each (Jezewska *et al.*, 1998c). Formation of the complex between the ssDNA 10-mer, $d\varepsilon A(p\varepsilon A)_9$, which binds exclusively to the strong subsite, and the DnaB helicase proceeds with the same mechanism as the binding of the 20-mer. Using the Smoluchowski equation, with $D_D = 1.8 \times 10^{-6}$ cm^2/second for the 10-mer, the theoretical value of the maximum rate constant for the diffusion-controlled association $k_D \sim 9.7 \times 10^9\ M^{-1}\ s^{-1}$. Thus, the determined bimolecular rate constant k_1 is about three to six orders of magnitude lower than the k_D predicted by the diffusion-controlled collision, strongly suggesting that, similar to the 20-mer, the bimolecular association step contains an additional conformational transition of the helicase-ssDNA 10-mer complex. Moreover, the largest increase of the 10-mer fluorescence in the complex with the DnaB helicase (largest conformational change) occurs in the formation of the $(H\text{-ssDNA})_1$, which excludes the possibility that this is a collision complex (see above). Therefore, the mechanism of the 10-mer binding to the DnaB helicase should include an additional step as described by Scheme 2.

The same mechanism of binding and the similar progress of the conformational transitions of the nucleic acid during the binding process indicate that the 10-mer forms all necessary contacts with the protein. These data agree well with equilibrium thermodynamic studies that show that crucial structural elements of the strong binding subsite are separated by no more than six or seven nucleotide residues (Jezewska *et al.*, 1998c). Moreover, the results indicate that only the strong binding subsite is on the main route in the recognition process of the ssDNA by DnaB. The role of the weak ssDNA-binding subsite seems to be passive in the dynamics of the ssDNA binding.

Comparison with other helicases

The kinetics of the DnaB helicase binding to the ssDNA is different from the dynamics of the ssDNA binding of an another well-studied *E. coli* Rep helicase. Rep protein is the only other helicase whose quantitative kinetic mechanism of interactions with a ssDNA has been determined directly (Lohman & Bjorson, 1996; Wong *et al.*, 1996; Bjorson *et al.*, 1996, 1998). Excellent, extensive kinetic data from Lohman's laboratory showed that the Rep helicase monomer binds ssDNA oligomers *via* a two-step mechanism, although some indication of the presence of an additional fast step, possibly following the collision step, has been indicated (Bjorson *et al.*, 1996, 1998). The determined bimolecular rate constant ($3 \times 10^7\ M^{-1}\ s^{-1}$) is close to the value expected for the diffusion-controlled reaction. However, rate constants for the subsequent step (3-8 s^{-1}) are similar to the values of k'_1 for the DnaB helicase (Scheme 2).

The Rep helicase exists in solution predominantly as a monomer that dimerizes upon complex formation with the DNA substrates (Lohman & Bjorson, 1996). In the case of the DnaB helicase, the enzyme forms a stable, ring-like structure in which protomer-protomer contacts are limited to two neighboring subunits (Bujalowski *et al.*, 1994; San Martin *et al.*, 1995; Yu *et al.*, 1996). Recently, we obtained evidence, using the fluorescence energy transfer approach, that in the complex with the helicase the ssDNA passes through the cross-channel of the hexamer (Jezewska *et al.*, 1998b). Similar structures of the enzymes and their complexes between a hexameric helicase and a ssDNA have been found in the case of bacteriophage T7 and T4 hexameric helicases (Dong *et al.*, 1995; Egelman *et al.*, 1995). Thus, the multi-step mechanism of the DnaB helicase binding to the ssDNA reflects the complex structure of its final equilibrium complex. At this point, it should be mentioned that binding of a ssDNA oligomer to the Rep dimer, already associated with another ssDNA oligomer, is characterized by a very low bimolecular rate constant (>250 s^{-1}), which certainly indicates a multiple-step process (Bjorson *et al.*, 1996, 1998).

Sequential character of the mechanism of the DnaB helicase binding to the ssDNA and its functional implications

Electron microscopy studies indicate that, in the presence of nucleotide cofactors (AMP-PNP and ADP), the DnaB hexamer can exist in two major conformations (Yu *et al.*, 1996). On the other hand, kinetics of the ligand binding is a very sensitive method to detect such pre-equilibrium conformational transitions of the macromolecule (Bernasconi, 1976; Bujalowski *et al.*, 1986a,b). For instance, if the DnaB hexamer exists in solution in an equilibrium of two conformational states prior to the ssDNA binding, and both states can bind the nucleic acid, then we should detect two relaxation times corresponding to the bimolecular binding steps to each conformation (Bernasconi, 1976). However, this is not what is experimentally observed (see above). Both relaxation times and amplitudes show behavior typical for the sequential mechanism of binding. On the other hand, if the DnaB hexamer exists in solution in different conformations in the presence of AMP-PNP, our data indicate that the equilibrium between these different states is very strongly shifted toward the conformation which strongly binds the ssDNA. The sequential mechanism indicates that, in the binding process, the ssDNA is not forced to select between different states of the enzyme complexed with the nucleotide cofactor.

Hydrodynamic studies showed that the DnaB hexameric structure is very stable in solution, with magnesium cations playing a specific role in maintaining its stability (Bujalowski *et al.*, 1994). As we pointed out, this stable hexameric structure and the structural role of Mg^{2+} cations distinguishes the DnaB helicase from other well-studied hexameric helicases for which the mechanism of binding to a ssDNA most probably includes oligomerization of the protein around the nucleic acid (Dong *et al.*, 1995; Egelman *et al.*, 1995; Hacker & Johnson, 1997). As determined in this work, the relaxation times for the 20-mer binding to the DnaB hexamer are independent of [DnaB] over approximately an order of magnitude of the enzyme concentration (Figure 6). The lack of the effect of the DnaB protein concentration on the relaxation time argues strongly against any dissociation of the DnaB hexamer prior to the ssDNA binding. Such large changes of the protein concentration would certainly affect any protein dissociation, if it occurred. In the final equilibrium complex, the ssDNA passes through the cross-channel of the DnaB hexamer (Jezewska *et al.*, 1998b). Therefore, in the initial stages of the reaction, the association of the DnaB hexamer with the ssDNA complex would include a collision complex, which is most probably followed by a transient and local opening of the hexamer.

The value of the determined rate constant k_1, for the formation of the $(H\text{-ssDNA})_1$ complex with the 20-mer and 10-mer, is $\sim 3 \times 10^4$-6×10^4 M^{-1} s^{-1} (Tables 1 and 2). On the other hand, the dissociation of the $(H\text{-ssDNA})_1$ back to the free helicase and the ssDNA is controlled by $k_{-1} \sim 0.02$-0.03 s^{-1}, which is about six orders of magnitude lower than the k_1, indicating that once the helicase forms the $(H\text{-ssDNA})_1$ with the ssDNA it is "locked" in the complex in a way that is largely independent of the nucleic acid length, base, and structure. These results strongly suggest that the local opening of the hexamer, possibly between only two subunits, and the entry of the ssDNA into the cross-channel of the hexamer occurs in the formation of the $(H\text{-ssDNA})_1$ complex, while subsequent transitions to $(H\text{-ssDNA})_2$ and $(H\text{-ssDNA})_3$ occur with the ssDNA already in the cross-channel of the hexamer. The large difference between the forward and backward rate constants for the first binding step and formation of the $(H\text{-ssDNA})_1$ is in contrast to similar values of the rate constants in the next steps (Tables 1 and 2).

Recall, the major conformational transition of the single-stranded nucleic acid-DnaB helicase complex occurs in the formation of the $(H\text{-ssDNA})_1$, which is an intrinsic conformational transition of the enzyme (see above). Also, the maximum increase of the ATPase activity of the enzyme by the ssDNA takes place within about three to five seconds after mixing the DnaB (1.5×10^{-7} M hexamer) with the $d\varepsilon A(p\varepsilon A)_{19}$ (5×10^{-6} M oligomer), final concentrations, in the same solution conditions as applied in the studies described here. Figure 12 shows the computer simulation of the time-courses of the fractional concentrations of the different DnaB intermediates in the association

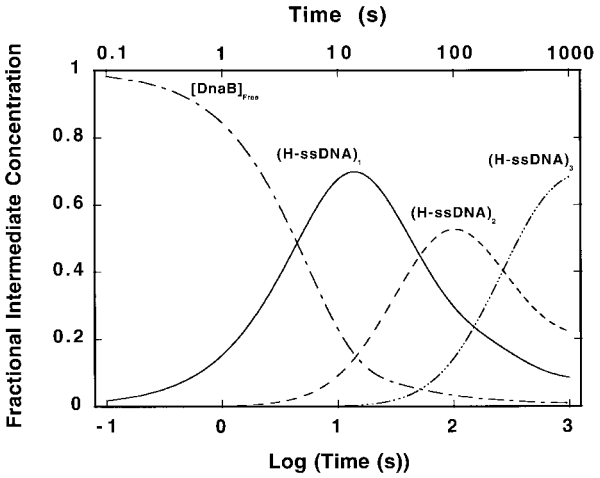

Figure 12. Computer simulation of the time-course of the fractional concentration distribution of different DnaB helicase species, in the binding of the 20-mer, $d\varepsilon A(p\varepsilon A)_{19}$, using the determined rate constants: $k_1 = 3.4 \times 10^4$ M^{-1} s^{-1}, $k_{-1} = 0.018$ s^{-1}, $k_2 = 0.021$ s^{-1}, $k_{-2} = 0.01$ s^{-1}, $k_3 = 0.004$ s^{-1}, and $k_{-3} = 0.0012$ s^{-1} (buffer T2 (pH 8.1, 100 mM NaCl, 1 mM AMP-PNP, 10 °C). The total DnaB and oligomer concentrations are 1.5×10^{-7} M (hexamer) and 5×10^{-6} M (oligomer), respectively; free DnaB (– – – – –), $(H\text{-ssDNA})_1$ (—), $(H\text{-ssDNA})_2$ (– – –), $(H\text{-ssDNA})_3$ (— – – – —).

reaction with the 20-mer, dεA(pεA)$_{19}$, in buffer T2 (pH 8.1, 100 mM NaCl, 1 mM AMP-PNP, 10 °C) using the same DnaB and 20-mer concentrations as those used in the ATPase assays and determined rate constants (Table 1). Thus, the dynamics of the ATPase-stimulated activity coincides with the time-course of the appearance of the (H-ssDNA)$_1$, suggesting that allosteric changes in the ATP-binding site, induced by the ssDNA, are already present in the (H-ssDNA)$_1$. The role of the different DnaB helicase-ssDNA complexes in the nucleic acid recognition, stimulating ATPase activity, and duplex DNA unwinding by the enzyme are currently being studied in our laboratory.

Materials and Methods

Reagents and buffers

All solutions were made with distilled and deionized >18 MΩ (Milli-Q Plus) water. All chemicals were reagent grade. Buffer T2 is 50 mM Tris adjusted to pH 8.1 with HCl, 5 mM $MgCl_2$, 10 % glycerol. The temperatures and concentrations of the NaCl and AMP-PNP in the buffer are indicated in the text.

DnaB protein

The *E. coli* DnaB protein was purified as described (Bujalowski & Klonowska, 1993, 1994a,b; Bujalowski *et al.*, 1994). The concentration of the protein was determined spectrophotometrically, using the extinction coefficient $\varepsilon_{280} = 1.85 \times 10^5$ cm^{-1} M^{-1} (Hexamer) (Bujalowski *et al.*, 1994).

Nucleic acids

Oligomers, dA(pA)$_{19}$, dA(pA)$_9$, dεA(pεA)$_4$(pT)$_{15}$ and dεA(pεA)$_4$(pA)$_{15}$ were purchased from Midland Certified Reagents (Midland, Texas). Oligomers were at least 95 % pure as judged by autoradiography on polyacrylamide gels. The etheno-derivatives of the dA(pA)$_{19}$ and dA(pA)$_9$ were obtained by modification with chloroacetaldehyde (Secrist *et al.*, 1972; Bujalowski & Jezewska, 1995; Rajendran *et al.*, 1998). This modification goes to completion and provides a fluorescent derivative of the ssDNA. The concentration of the etheno-derivative of the nucleic acids was determined using the extinction coefficient 3700 M^{-1} cm^{-1} (nucleotide) at 257 nm (Ledneva *et al.*, 1977).

Fluorescence measurements

Steady-state fluorescence titrations were performed using the SLM-AMINCO 48000S or 8100 spectrofluorometers. In order to avoid possible artifacts due to the fluorescence anisotropy of the sample, polarizers were placed in excitation and emission channels and set at 90° and 55° (magic angle), respectively (Jezewska & Bujalowski, 1996a; Jezewska *et al.*, 1996). The binding was followed by monitoring the fluorescence of the etheno-derivatives (Jezewska *et al.*, 1996, 1998c). The fractional fluorescence change, ΔF_i, is defined as $\Delta F_i = (F_i - F_0)/F_0$ where F_i is the fluorescence emission of the ssDNA etheno-derivative, at a given DnaB concentration, and F_0 is the initial value of the nucleic acid fluorescence.

Stopped-flow kinetics

All fluorescence stopped-flow kinetic experiments were performed using either the SX.MV18 or the SX.MV18 sequential stopped-flow instrument (Applied Photophysics Ltd, Leatherhead, UK). The reactions were monitored using the fluorescence of the etheno-derivatives of the ssDNA oligomers with $\lambda_{ex} = 320$ nm, and emission observed through a GG400 cutoff filter (Schott, PA), with the excitation monochromator slits at 1 mm (band pass ~4.5 nm). The small excitation slits were used to limit photo-bleaching of the sample during long-time scans. The experiments were performed in the ''oversampling'' mode, in which the instrument collects and averages the multiple data points at the fastest instrumental rate for the selected time interval, achieving a higher signal to noise ratio. Usually, three to eight traces were collected and averaged for each sample. The kinetic curves were fitted to extract relaxation times and amplitudes using non-linear least-squares software provided by the manufacturer, with the exponential function defined as:

$$F(t) = F(\infty) + \sum_{i=1}^{n} A_i \exp(-\lambda_i t) \qquad (26)$$

where $F(t)$ is the fluorescence intensity at time t, $F(\infty)$ is the fluorescence intensity at $t = \infty$, A_i is the amplitude corresponding to the ith relaxation process, λ_i is the time constant (reciprocal relaxation time) characterizing the ith relaxation process, and n is the number of relaxation processes. All further analyses of the data were performed using Mathematica (Wolfram, Urbana, IL) and KaleidaGraph (Synergy Software, PA) on MacIntosh G3 computers.

Acknowledgments

We thank Gloria Drennan Davis for her help in preparing the manuscript. This work was supported by NIH grants GM-46679 and GM-58565 (to W. B.).

References

Arai, K. & Kornberg, A. (1981). Mechanism of dnaB protein action. Allosteric role of ATP in the alteration of DNA structure by dnaB protein in priming replication. *J. Biol. Chem.* **256**, 5260-5266.

Baker, B. M., Vanderkooi, J. & Kallenbach, N. R. (1978). Base stacking in a fluorescent dinucleotiside monophosphate: εApεA. *Biopolymers*, **17**, 1361-1372.

Baker, T. A., Funnell, B. E. & Kornberg, A. (1987). Helicase action of dnaB protein during replication from the *Escherichia coli* chromosomal origin *in vitro*. *J. Biol. Chem.* **262**, 6877-6885.

Bernasconi, C. F. (1976). *Relaxation Kinetics*, Academic Press, New York.

Berry, R. S., Rice, S. A. & Ross, J. (1980). Chemical kinetics. In *Physical Chemistry*, chapt. 30, J. Wiley & Sons, New York.

Bjorson, K. P., Moore, K. J. & Lohman, T. M. (1996). Kinetics mechanism of DNA binding and DNA-induced dimerization of the *Escherichia coli* Rep helicase. *Biochemistry*, **35**, 2268-2282.

Bjorson, K. P., Hsieh, J., Amaratunga, M. & Lohman, T. M. (1998). Kinetic mechanism for the sequential

binding of two single-stranded oligodeoxynucleotides to the *Escherichia coli* Rep helicase dimer. *Biochemistry,* **37**, 891-899.

Bujalowski, W. & Jezewska, M. J. (1995). Interactions of *Escherichia coli* primary replicative helicase DnaB protein with single-stranded DNA. The nucleic acid does not wrap around the protein hexamer. *Biochemistry,* **34**, 8513-8519.

Bujalowski, W. & Klonowska, M. M. (1993). Negative cooperativity in the binding of nucleotides to *Escherichia coli* replicative helicase DnaB protein. Interactions with fluorescent nucleotide analogs. *Biochemistry*, **32**, 5888-5900.

Bujalowski, W. & Klonowska, M. M. (1994a). Structural characteristics of the nucleotide binding site of the *E. coli* primary relicative helicase DnaB protein. Studies with ribose and base-modified fluorescent nucleotide analogs. *Biochemistry,* **33**, 4682-4694.

Bujalowski, W. & Klonowska, M. M. (1994b). Close proximity of tryptophan residues and ATP-binding site in *Escherichia coli* primary replicative helicase DnaB protein. Molecular topography studies. *J. Biol. Chem.* **269**, 31359-31371.

Bujalowski, W., Greaser, E., McLaughlin, L. W. & Porschke, D. (1986a). Anticodon loop of $tRNA^{Phe}$: structure, dynamics, and Mg^{2+} binding. *Biochemistry,* **25**, 6365-6378.

Bujalowski, W., Jung, M., McLaughlin, L. W. & Porschke, D. (1986b). Codon-induced association of the isolated anticodon loop of $tRNA^{Phe}$. *Biochemistry,* **25**, 6372-6371.

Bujalowski, W., Klonowska, M. M. & Jezewska, M. J. (1994). Oligomeric strucutre of *Escherichia coli* primary replicative helicase DnaB protein. *J. Biol. Chem.* **269**, 31350-31358.

Dong, F., Gogol, E. P. & von Hippel, P. H. (1995). The phage T4-coded DNA replication helicase (gp41) forms a hexamer upon activation by nucleoside triphosphate. *J. Biol. Chem.* **270**, 7462-7473.

Egelman, E. H., Yu, X., Wild, R., Hingorani, M. M. & Patel, S. S. (1995). Bacteriphage T7 helicase/primase proteins form rings around single-stranded DNA that suggest a general structure for hexameric helicases. *Proc. Natl Acad. Sci. USA,* **92**, 3869-3873.

Fraser, R. A., Duncan, W. J. & Collar, A. R. (1965). Lambda-matrices and canonical forms. In *Elementary Matrices and Some Applications to Dynamics and Differential Equations*, chapt. 3, Cambridge University Press, Cambridge.

Hacker, K. J. & Johnson, K. A. (1997). A hexameric helicase encircles one DNA strand and excludes the other during DNA unwinding. *Biochemistry,* **36**, 14080-14087.

Jezewska, M. J. & Bujalowski, W. (1996a). A general method of analysis of ligand binding to competing macromolecules using the spectroscopic signal originating from a reference macromolecule. Application to *Escherichia coli* replicative helicase DnaB protein-nucleic acid interactions. *Biochemistry,* **35**, 2117-2128.

Jezewska, M. J. & Bujalowski, W. (1996b). Global conformational transitions in *E. coli* primary replicative DnaB protein induced by ATP, ADP and single-stranded DNA binding. *J. Biol. Chem.* **271**, 4261-4265.

Jezewska, M. J., Kim, U.-S. & Bujalowski, W. (1996). Binding of *Escherichia coli* primary replicative helicase DnaB protein to single-stranded DNA. Long-range allosteric conformational changes within the protein hexamer. *Biochemistry,* **36**, 2129-2145.

Jezewska, M. J., Rajendran, S. & Bujalowski, W. (1997). Strand specificity in the interactions of *Escherichia coli* primary replicatve helicase DnaB protein with replication fork. *Biochemistry,* **36**, 10320-10326.

Jezewska, M. J., Rajendran, S. & Bujalowski, W. (1998a). Complex of *Escherichia coli* primary replicative helicase DnaB protein with a replication fork. Recognition and structure. *Biochemistry,* **37**, 3116-3136.

Jezewska, M. J., Rajendran, S., Bujalowska, D. & Bujalowski, W. (1998b). Does ssDNA pass through the inner channel of the protein hexamer in the complex with the *E. coli* DnaB helicase? Fluorescence energy transfer studies. *J. Biol. Chem.* **273**, 10515-10529.

Jezewska, M. J., Rajendran, S., Bujalowska, D. & Bujalowski, W. (1998c). Functional and structural heterogeneity of the DNA binding of the *E. coli* primary replcative helicase DnaB protein. *J. Biol. Chem.* **273**, 9058-9069.

Kornberg, A. & Baker, T. A. (1992). DNA helicases. In *DNA Replication*, chapt. 11, Freeman, San Francisco.

LeBowitz, J. H. & McMacken, R. (1986). The *Escherichia coli* dnaB replication protein is a DNA helicase. *J. Biol. Chem.* **261**, 4738-4748.

Ledneva, R. K., Razjivin, A. P., Kost, A. A. & Bogdanov, A. A. (1977). Interaction of tobacco mosaic virus protein with synthetic polynucleotides containing a fluorescent label: optical properties of poly(A,εA) and poly(C,εC) copolymers and energy migration from the tryptophan to $1,N^6$-ethenoadenosine or $3,N^4$-ethenocytosine residues in RNP. *Nucl. Acids Res.* **5**, 4226-4243.

Lohman, T. M. & Bjorson, K. P. (1996). Mechanisms of helicase-catalyzed DNA unwinding. *Annu. Rev. Biochem.* **65**, 169-214.

Moore, J. W. & Pearson, R. G. (1981). Reaction in solution. In *Kinetics and Mechanism*, chapt. 7, J. Wiley & Sons, New York.

Mulsch, A., Colpan, M., Wollny, E., Gassen, H. G. & Riesner, D. (1981). Mechanism of the interactions between ribosomal protein S1 and oligonucleotides. *Nucl. Acids Res.* **9**, 2367-2385.

Pilar, F. L. (1968). Introduction to matrix theory. In *Elementary Quantum Chemistry*, chapt. 9, McGraw-Hill, New York.

Porschke, D. (1973). The dynamics of nucleic-acid single-strand conformation changes. *Eur. J. Biochem.* **39**, 117-126.

Porschke, D. (1976). The nature of stacking interactions in polynucleotides. Molecular states in oligo- and polyribocytidylic acids by relaxation analysis. *Biochemistry,* **15**, 1495-1499.

Porschke, D. (1978). Molecular states in single-stranded adenylate chains by relaxation analysis. *Biopolymers,* **17**, 315-232.

Rajendran, S., Jezewska, M. J. & Bujalowski, W. (1998). Human DNA polymerase β recognizes single-stranded DNA using two different binding modes. *J. Biol. Chem.* **273**, 31021-31031.

Saenger, W. (1984). Synthetic homopolymer nucleic acids structures. In *Principles of Nucleic Acid Structure*, chapt. 13 edit., .

San, Martin M. C., Stamford, N. P. J., Dammerova, N., Dixon, N. E. & Carazo, J. M. (1995). A structural model for the *Escherichia coli* DnaB helicase based on electron microscopy data. *J. Struct. Biol.* **114**, 167-176.

Secrist, J. A., Bario, J. R., Leonard, N. J. & Weber, G. (1972). Fluorescent modification of adenosine-containing coenzymes. Biological activities and spectroscopic properties. *Biochemistry*, **11**, 3499-3506.

Tanford, C. (1961). *Physical Chemistry of Macromolecules*, J. Wiley, New York.

Tolman, G. L., Barrio, J. R. & Leonard, N. J. (1974). Chloroacetaldehyde-modified dinucleoside phosphates. Dynamic fluorescence quenching and quenching due to intramolecular complexation. *Biochemistry*, **13**, 4869-4878.

Wong, I., Moore, K. J., Bjorson, K. J., Hsieh, J. & Lohman, T. M. (1996). ATPase activity of *Escherichia coli* Rep helicase is dramatically dependent on DNA ligation and protein oligomeric state. *Biochemistry*, **35**, 5726-5734.

Yu, X., Jezewska, M. J., Bujalowski, W. & Egelman, E. H. (1996). The hexameric *E. coli* DnaB helicase can exist in different quaternary states. *J. Mol. Biol.* **259**, 7-14.

Edited by D. E. Draper

(Received 20 September 1999; received in revised form 8 November 1999; accepted 11 November 1999)